



Wet torrefaction of biomass waste into levulinic acid and high-quality hydrochar using H-beta zeolite catalyst

Andrii Kostyniuk^{a,*}, Blaž Likozar^{a,b,c,d}

^a Department of Catalysis and Chemical Reaction Engineering, National Institute of Chemistry, Hajdrihova 19, Ljubljana, 1001, Slovenia

^b Faculty of Polymer Technology, Slovenj Gradec 2380, Slovenia

^c Pulp and Paper Institute, Bogišičeva 8, Ljubljana 1000, Slovenia

^d Faculty of Chemistry and Chemical Technology, University of Ljubljana, Večna Pot 113, Ljubljana 1000, Slovenia

ARTICLE INFO

Handling Editor: Panos Seferlis

Keywords:

Biomass waste
Cellulose
Hydrochar
Levulinic acid
Wet torrefaction

ABSTRACT

Wet torrefaction (WT) is an effective pretreatment method of biomass waste for producing high-quality hydrochar and valuable liquid products. This study delves into how acid catalysts and reaction conditions in WT impact the resulting hydrochar's surface characteristics and elemental composition, as well as the distribution of liquid products. The focus is on utilizing wood cellulose pulp residue (WCPR) as the feedstock with H-Beta zeolite catalyst in a nitrogen-rich environment. The WT process involves a temperature range of 180–260 °C, and reaction durations spanning 15–60 min. The findings reveal that WT conditions, including the catalyst for WCPR, significantly influence the hydrochar's properties and liquid product distribution. With increasing temperature and reaction time, the hydrochar experiences changes, including increased carbon content and reduced oxygen content. The study identifies 260 °C and 30 min as the optimal temperature and time for levulinic acid production, achieving a remarkable selectivity of 62.8% with the H-Beta zeolite catalyst using H₂O/WCPR = 10. Various properties of the resulting hydrochar are assessed, including higher heating values (HHVs), decarbonization (DC), dehydrogenation (DH), deoxygenation (DO), enhancement factor, carbon enrichment, surface area, pore diameter, weight loss as well as solid, carbon, hydrogen, and energy yields. The WT + Beta 220 sample, processed at 220 °C for 30 min, exhibited the highest HHV at 30.3 MJ/kg and carbon content at 78.9% in hydrochar compared to various biomass types, with an enhancement factor of 1.51 and carbon enrichment of 1.63, while the sequence of element removal during WT prioritized as DO > DH > DC. Furthermore, it is worth highlighting that the most significant weight loss, increasing from 17.0 to 60.7%, was observed under the same WT conditions. Lastly, a comprehensive reaction pathway is proposed to elucidate the WT of WCPR with the presence of H-Beta zeolite catalyst under these optimized conditions.

1. Introduction

Addressing the escalating energy crisis and environmental concerns is of paramount importance for sustaining modern society (Gan et al., 2020). The conventional practice of burning non-renewable fossil fuels like petroleum, coal, and natural gas for heat and energy production, while pivotal for human civilization, poses significant environmental hazards and is poised to run out within the next few decades (Saha et al., 2022). As a solution to these pressing issues, biomass emerges as a promising alternative. Biomass can undergo various thermochemical conversion technologies to yield solid, liquid, and gaseous biofuels, providing a sustainable and eco-friendly energy source (Niu et al., 2022).

Biomass, known for its near carbon-neutral properties and abundant availability in nature, offers the potential to substantially decrease fossil fuel consumption and environmental pollution, particularly in reducing greenhouse gas emissions (Wang et al., 2018). Cellulose, hemicelluloses, and lignin form the principal constituents of lignocellulosic biomass, accompanied by minimal amounts of organic extractives and inorganic minerals. In the majority of lignocellulosic biomass, these three components typically make up more than 90% of the total weight (Chen et al., 2021). Biomass, ranking as the fourth most significant global energy source after coal, oil, and natural gas, represents a crucial and easily accessible form of renewable energy in today's energy landscape (Kota et al., 2022). Nonetheless, biomass faces limitations compared to

* Corresponding author. Department of Catalysis and Chemical Reaction Engineering, National Institute of Chemistry, Hajdrihova 19, SI-1000 Ljubljana, Slovenia.
E-mail addresses: andrii.kostyniuk@ki.si, andry_kost@ukr.net (A. Kostyniuk).

<https://doi.org/10.1016/j.jclepro.2024.141735>

Received 14 January 2024; Received in revised form 29 February 2024; Accepted 9 March 2024

Available online 13 March 2024

0959-6526/© 2024 The Authors. Published by Elsevier Ltd. This is an open access article under the CC BY license (<http://creativecommons.org/licenses/by/4.0/>).

coal, such as a lower calorific value, higher moisture content, hydrophilic nature, poor grindability, handling, storage, and lower energy density in comparison to fossil fuels, which impact its viability as an alternative to conventional energy sources, and combustion of biomass is highly inefficient and expensive (Sarvaramini et al., 2013). Hence, to address this limitation and produce biofuels of high density, thermochemical conversion processes are essential.

Thermochemical conversion processes, such as torrefaction, pyrolysis, hydrothermal liquefaction, gasification, and combustion, represent prevalent techniques for transforming biomass into valuable energy forms (Kwoczyński and Čmelík, 2021). Among these methods, torrefaction, considered a mild pyrolysis method, stands out as a significant process primarily employed in the production of solid biofuel, also known as biochar or hydrochar (Chen et al., 2021; Lin et al., 2021). Hydrochar has established itself as a versatile material, known for its diverse applications. Depending on its surface properties, structure, and composition, modified hydrochar finds utility in various domains such as greenhouse gas sequestration, cost-effective adsorbents, soil enhancement, catalyst support, and more (Zhu et al., 2019). Torrefied biomass shares similar properties with coal and can serve as a partial substitute for coal (Ong et al., 2020; Tong et al., 2018). Following torrefaction, biomass can undergo densification, typically through briquetting or pelletizing using standard densification equipment, effectively enhancing material density and enhancing its hydrophobic characteristics (Sukiran et al., 2017).

Torrefaction is a mild pyrolysis process applied to biomass for thermal pretreatment, with the goal of improving its higher heating values and energy densities, lowering atomic O/C and H/C ratios, reducing moisture content, enhancing water resistance, increasing grindability and reactivity, and achieving uniform properties (Leontiev et al., 2018). Conventional torrefaction or dry torrefaction (DT), conducted in an oxygen-free environment, typically involves low heating rates, generally below 50 °C per min, and occurs within a temperature range of 200–300 °C with durations of 15–60 min (Rodríguez-Alejandro et al., 2023; Zhang et al., 2022). Wet torrefaction (WT), often referred to as hydrothermal torrefaction, is a high-pressure (2–10 MPa) thermal pretreatment process conducted in hot compressed water under inert conditions, typically at temperatures ranging from 180 to 260 °C with a short reaction time (5–60 min) (Bach et al., 2017; Srisang et al., 2022). This method has received considerable recognition as an effective approach for pre-treating high-moisture or extremely wet biomass, obviating the requirement for a separate drying step (Zhang et al., 2017).

In comparison to DT, WT not only achieves higher thermal efficiency and reduces pollutant emissions but also improves the heating value, energy density, hydrophobicity, and grindability of biomass feedstocks (He et al., 2021). In the liquid environment of WT, intricate chemical reactions take place, allowing for the achievement of diverse extraction efficiencies for both organic and inorganic components under the ideal WT conditions. Since water remains in a liquid phase during WT, this process helps prevent energy loss in the form of latent heat resulting from water vaporization (Bach et al., 2017).

As torrefaction temperature rises, there is a decrease in the mass yield and volatile content of solid products, accompanied by an increase in fixed carbon and ash content. Moreover, the influence of residence time on the properties of solid products during torrefaction is more pronounced at higher temperatures, and the composition of the torrefaction atmosphere can also impact the physicochemical characteristics and combustion/pyrolysis properties of the resulting products (Li et al., 2020). Throughout the torrefaction process, the chemical composition of biomass undergoes alteration, leading to the substantial reduction of oxygen content and an elevation in calorific value (Tong et al., 2018). In particular, WT preserves active hydroxyl groups through macromolecular structural rearrangement, promoting a more organized cellulose structure (Zhu et al., 2019).

Levulinic acid, a versatile renewable platform molecule with various potential industrial applications, forms the basis for producing a diverse

range of high-volume chemicals and fuels (Weingarten et al., 2012). It finds applications in pharmaceuticals, where it serves as a building block for drug molecules, as well as in agrochemicals and polymers, contributing to the development of renewable and biodegradable materials. Hydrochar, on the other hand, represents a renewable solid fuel with potential applications in energy production and carbon sequestration. Its porous structure and high carbon content make it suitable for use in combustion processes, offering a cleaner alternative to traditional fossil fuels. Additionally, hydrochar can be utilized as a soil amendment to improve soil fertility, water retention, and carbon storage, contributing to sustainable agriculture and land management practices. Levulinic acid production can be accomplished in a single step by dehydrating cellulose with an acid catalyst, with 5-HMF serving as an intermediate. The most significant levulinic acid yields, up to 75%, have been obtained when using sulfuric acid in aqueous solutions (Alonso et al., 2013). The use of sulfuric acid, and mineral acids in general, as homogeneous acid catalysts in the commercial production of levulinic acid presents a primary drawback. It necessitates the separation of the mineral acid from the reaction product, which can have adverse effects on subsequent processes, such as the production of γ -valerolactone. This reliance on sulfuric acid contributes to heightened production costs due to its expense, the requirement for neutralization, and the associated challenges in separating it from levulinic acid (Alonso et al., 2013; Weingarten et al., 2012).

Recyclable solid acid catalysts have been employed in attempts to produce levulinic acid from biomass feedstocks. Xu and their colleagues (Xu et al., 2023) acquired levulinic acid from cellulose through the application of a carbon foam-supported heteropolyacid catalyst. This approach resulted in a remarkable cellulose conversion rate of 89.4% and a levulinic acid yield of 60.9% at a reaction temperature of 180 °C for a duration of 4 h, using a stainless steel reactor. In a different approach, Xiang and his co-workers (Xiang et al., 2017) employed ETS-10 zeolite and achieved a substantial levulinic acid yield of 91.0% while conducting the reaction in an atmosphere of H₂. Meanwhile, Weingarten et al. (2012) effectively transformed cellulose into levulinic acid by utilizing Amberlyst 70 as a catalyst at a temperature of 220 °C over a 30 min duration. This procedure yielded a maximum of 28% levulinic acid, which amounted to 28% of the theoretical yield, when conducted in reactor vessels of both 100 and 160 mL capacities. These vessels were operated in a helium atmosphere under a pressure of 4–5 MPa. In a subsequent study, Chen and co-workers (Chen et al., 2017) used Amberlyst 36 as the catalyst within a temperature range spanning 120–150 °C, significantly expediting the production of levulinic acid. They managed to achieve yields between 13 and 17% in a mere 5 min, harnessing microwave heating as their method. In a different study, Wang and colleagues (Wang et al., 2018) employed sulfonated humins in a sulfonated water solution as a catalyst, successfully transforming cellulose into levulinic acid with a yield of 65.9%.

In this research study, the focus was on WT applied to wood cellulose pulp residue (WCPR). WCPR is the leftover material that remains after extracting cellulose fibers from wood, a process achieved through physical, chemical, or biological methods, commonly used in several industrial sectors, particularly in the paper and pulp industry (Zhang et al., 2023). This residual material consists of various wood components that do not get transformed into cellulose fibers during the pulping process. Recent data provided by Statista (Statista Research Department, 2023) reveals a consistent and robust performance in the global pulp industry, with production consistently exceeding 180 million metric tons on an annual basis for the past decade. In 2022, the global production of wood pulp experienced a notable surge, reaching over 195.79 million metric tons.

In the ongoing research, the investigation began with subjecting WCPR to a WT process within a batch reactor. This involved employing an H-Beta zeolite catalyst in the presence of water as the reaction medium. A comprehensive examination of several reaction parameters was carried out, encompassing factors such as reaction time, temperature,

and the amount of catalyst. The primary objective of this extensive examination was to pinpoint the most favorable conditions for the conversion of WCPR into high-quality hydrochar and value-added products, with a specific focus on maximizing the yield of levulinic acid. Levulinic acid is included among the twelve bio-based platform chemicals utilized in the manufacture of chemicals, polymers, and biofuels, and its production can be achieved by subjecting biomass to acid hydrolysis (Chen et al., 2017).

Furthermore, the study aimed to elucidate the potential mechanisms involved in the transformation of cellulose into levulinic acid. Additionally, a comprehensive analysis was performed on the WCPR and the hydrochar produced during the WT process. Various techniques for characterizing these materials, such as X-ray diffraction (XRD), scanning electron microscopy (SEM), Brunauer-Emmett-Teller analysis (BET), elemental analysis of carbon, hydrogen, nitrogen, oxygen, and sulfur (CHN(O)S), as well as thermogravimetric analysis (TGA), were employed for this purpose. These analyses yielded valuable insights into the structural and compositional features of the hydrochar. In this investigation, an innovative chemocatalytic method was proposed, employing H-Beta zeolite catalysts in a batch reactor under a nitrogen atmosphere. The aim was to simultaneously generate value-added products, such as levulinic acid, from WCPR during WT conversion, while also producing high-quality solid fuel. These findings underscore the significance of WT as a promising approach for sustainable biomass utilization, offering potential benefits to both society and industry. From a societal perspective, the study contributes to the development of renewable energy sources and addresses environmental concerns by providing an alternative to fossil fuels. For industry, WT presents opportunities for the production of high-value chemicals from biomass waste streams, contributing to economic growth and sustainability efforts.

2. Experimental section

2.1. Materials

The H-Beta zeolite catalyst, featuring a $\text{SiO}_2/\text{Al}_2\text{O}_3$ ratio of 28, was procured from the commercial supplier Tosoh Corporation. This zeolite catalyst underwent a calcination process at $550\text{ }^\circ\text{C}$ ($10\text{ }^\circ\text{C}/\text{min}$) in the air for 6 h to remove impurities before being used in the study. All chemical reagents, calibration standards, and gases were commercially sourced and used without the need for further purification. The specific chemicals and their respective suppliers are listed as follow: levulinic acid (99.5%, Sigma Aldrich), 5-hydroxymethylfurfural (>97 wt%, Carbo-synth, reference number FH10853), 5-methylfurfural (99 wt%, Sigma Aldrich), furfural (>99 wt%, Sigma Aldrich), ethanol (>99.8%, Sigma Aldrich), methanol (>99.9%, Sigma Aldrich), hydroxyacetone (99.5%, Sigma Aldrich), guaiacol (99.5%, Sigma Aldrich), 2,3-butanedione (99%, Sigma Aldrich), phenol ($\geq 98.5\%$, Sigma Aldrich), 2-butanone (99.5%, Sigma Aldrich), acetone (>99.5%, Sigma Aldrich), acetoin (>99.5%, Sigma Aldrich), acetic acid (>99.7%, Sigma Aldrich), cyclopentenone (>99%, Sigma Aldrich), acetylacetone (>99%, Sigma Aldrich), 2,5-hexanedione (>99.5%, Sigma Aldrich), hydrogen (5.0, Messer, Germany), nitrogen (5.0, Messer, Germany), helium (5.0, Messer, Germany). The feedstock, referred to as WCPR (wood cellulose pulp residue), was sourced from the biotechnology company Vertoro (Geleen, Netherlands). A detailed composition of WCPR can be found in Table S1.

2.2. Proximate and ultimate analysis

The moisture, volatile matter, fixed carbon, and ash content in the untreated and wet torrefied wood cellulose pulp residue were determined through proximate analysis using a thermal gravimetric analyzer (specifically, the Spectrum 3 with EGA 4000 from PerkinElmer). The assessment of moisture, ash, and volatile matter utilized the E-871, E-

1755, and E-872 standards from the American Society for Testing and Materials (ASTM) (García et al., 2013; Li et al., 2021). In this analysis, about 10 mg of the sample was exposed to a controlled heating process within a nitrogen atmosphere. The process initiated at $40\text{ }^\circ\text{C}$ and progressed to $120\text{ }^\circ\text{C}$, with a 10 min pause for measuring the moisture content (M, %). Following this, a heating rate of $50\text{ }^\circ\text{C}/\text{min}$ was applied until $800\text{ }^\circ\text{C}$, and a 20 min hold was instituted to gauge the volatile matter (VM, %). To ascertain the ash content (Ash, %), the cooling phase commenced with a cooling rate of $-50\text{ }^\circ\text{C}/\text{min}$ until reaching $450\text{ }^\circ\text{C}$, at which point the nitrogen atmosphere was replaced with air. Subsequently, a new heating ramp of $25\text{ }^\circ\text{C}/\text{min}$ was initiated, continuing until $800\text{ }^\circ\text{C}$, and then maintained isothermally for 3 min. The fixed carbon content (FC, %) was calculated by using Equation (2) below.

$$\text{FC} = 100 - (\text{M} + \text{Ash} + \text{VM}). \quad (1)$$

The CHNS elemental analyzer vario EL cube (Elementar, Hanau, Germany) was employed in CHNS mode, with carbon, hydrogen, nitrogen, and sulfur contents determined. Carbon, hydrogen, and nitrogen levels were ascertained using a thermal conductivity detector, while sulfur content was measured using an infrared detector. The limit of detection (LOD) were determined to be 0.11%. Additionally, the standard deviation (SD) associated with the measurements was found to be 0.01%. To calibrate the instrument, a low-level standard containing 67.65% C, 4.95% H, 0.72% N, and 0.84% S, available from Elementar, was utilized. The combustion and reduction tubes were set to temperatures of $1150\text{ }^\circ\text{C}$ and $850\text{ }^\circ\text{C}$, respectively. The CHNOS content was ultimately evaluated on a dry basis by subtracting the water content.

$$\text{O} = 100\% - \text{C}\% - \text{H}\% - \text{N}\% - \text{S}\% - \text{moisture}\% - \text{Ash}\% - \text{Si}\% - \text{Al}\% \quad (2)$$

2.3. WCPR and WT + Beta samples characterization

Nitrogen adsorption at the temperature of liquid nitrogen (77 K) was carried out with the aid of a Micromeritics micropore analyzer (specifically, the Micromeritics ASAP, 2020 instrument) (Kostyniuk et al., 2020). This analysis aimed to ascertain the BET surface area for both the untreated and moistened torrefied samples. Additionally, a high-resolution scanning electron microscopy (HR-SEM) examination was conducted on WCPR and wet torrefied WCPR samples, employing the FE-SEM SUPRA 35-VP instrument produced by Carl Zeiss (Kostyniuk et al., 2020).

X-ray diffraction (XRD) analysis was performed using a PANalytical XpertPro powder X-ray diffraction instrument. $\text{CuK}\alpha 1$ radiation with a wavelength of 1.54056 \AA was applied at 45 kV and 40 mA within a scanning range of $5\text{--}50^\circ$, with increments of 0.033° (Kostyniuk et al., 2022). A TGA-IR (thermogravimetric analysis-infrared spectrometry) Spectrum 3 with EGA 4000 from PerkinElmer was employed to investigate the pyrolysis of dried and torrefied cellulose. Each test utilized approximately 10 mg of sample, which was subjected to heating from 40 to $750\text{ }^\circ\text{C}$ at a rate of $10\text{ }^\circ\text{C}/\text{min}$. A carrier gas of nitrogen (purity >99.999%) with a flow rate of 20 mL/min was used, and the experimental results of TGA were automatically recorded by a computer.

2.4. H-Beta catalyst characterization

H-Beta zeolite, known for its high acidity and porous structure, is selected as the catalyst due to its potential to facilitate dehydration reactions and promote the formation of desired chemical products during wet torrefaction. By leveraging the catalytic properties of H-Beta zeolite, the aim was to enhance the efficiency and selectivity of the wet torrefaction process for WCPR. Through systematic experimentation and analysis, the aim was to elucidate the role of H-Beta zeolite in catalyzing biomass conversion reactions and improving the overall performance of wet torrefaction. The structural characteristics of the H-Beta zeolite catalyst were determined through various methods, and the results are outlined in Table S2. The acid properties of the H-Beta zeolite are

presented in Table S3 and were examined using temperature-programmed desorption of ammonia (NH₃-TPD). This analysis was conducted utilizing a Micromeritics Autochem 2920 II apparatus equipped with a Pfeiffer Vacuum Thermostar quadrupole mass spectrometer. Additionally, pyridine adsorption diffuse-reflection infrared spectroscopy (Pyridine-DRIFTS) was performed using a Frontier IR spectrometer (PerkinElmer) equipped with an MCT detector and a Dif-fusIR® accessory from Pike Scientific (Kostyniuk et al., 2021a).

2.5. Calculations

The higher heating value (HHV) for both the untreated and wet torrefied cellulose pulp residue was determined using Equation (3) (Wu et al., 2023):

$$\text{HHV (MJ/kg)} = 0.3491 \times C + 1.1783 \times H - 0.1034 \times O + 0.1005 \times S - 0.0151 \times N - 0.0211 \times \text{Ash} \quad (3)$$

In this equation, C, H, O, S, N, and A denote the carbon, hydrogen, oxygen, sulfur, nitrogen, and ash contents, respectively, which were derived from the elemental analysis and expressed as weight percentages on a dry basis. By employing these equations, it becomes possible to compute both the higher and lower heating values of the biomass. This, in turn, provides a comprehensive insight into the energy characteristics of the biomass under torrefaction conditions.

The formulas utilized to calculate the solid yield and energy yield of the torrefied samples were as follows:

$$Y_{\text{solid}} = (m_{\text{product}} / m_{\text{feedstock}}) \times 100\% \quad (4)$$

$$Y_{\text{energy}} = ((Y_{\text{solid}} \times \text{HHV}_{\text{product}}) / \text{HHV}_{\text{feedstock}}) \times 100\% \quad (5)$$

In these equations, Y_{solid} stands for the solid yield, and Y_{energy} represents the energy yield. The variables $m_{\text{feedstock}}$ and m_{product} denote the mass of the starting samples and the solid product after torrefaction, respectively. $\text{HHV}_{\text{feedstock}}$ and $\text{HHV}_{\text{product}}$ indicate the higher heating value (in MJ/kg) of the original samples and the solid product after torrefaction, respectively (Chen et al., 2018).

Enhancement factor was defined as follows (Zhang et al., 2018):

$$\text{Enhancement factor} = \text{HHV}_{\text{product}} / \text{HHV}_{\text{feedstock}} \quad (6)$$

Carbon yield (Y_C) and hydrogen yield (Y_H) were calculated as follow (Wang et al., 2018):

$$Y_C (\%) = Y_{\text{solid}} (\%) \times (C_{\text{product}} / C_{\text{feedstock}}) \quad (7)$$

$$Y_H (\%) = Y_{\text{solid}} (\%) \times (H_{\text{product}} / H_{\text{feedstock}}) \quad (8)$$

where C_{product} , H_{product} and $C_{\text{feedstock}}$, $H_{\text{feedstock}}$ are the dry ash free carbon and hydrogen content of the WT + Beta and WCPR samples, respectively.

Decarbonization (DC), dehydrogenation (DH), and deoxygenation (DO), or oxygen removal efficiency (ORE), are three metrics utilized to quantify the reduction in mass of carbon, hydrogen, and oxygen during biomass torrefaction (Zhang et al., 2018). DC indicates the proportion of carbon loss in the biomass as a result of wet torrefaction and can be calculated using the following formula:

$$\text{DC} (\%) = 100 - Y_{\text{solid}} (\%) \times (C_{\text{product}} / C_{\text{feedstock}}) \quad (9)$$

DH and DO can be similarly calculated using the same procedure as DC.

$$\text{DH} (\%) = 100 - Y_{\text{solid}} (\%) \times (H_{\text{product}} / H_{\text{feedstock}}) \quad (10)$$

$$\text{DO} (\%) = 100 - Y_{\text{solid}} (\%) \times (O_{\text{product}} / O_{\text{feedstock}}) \quad (11)$$

where O_{product} and $O_{\text{feedstock}}$ are the dry ash free oxygen content of the WT + Beta and WCPR samples, respectively.

A metric referred to as carbon enrichment (CE), used to assess the degree of carbonization in WT + Beta, is defined as follows:

$$\text{CE} = C_{\text{product}} / C_{\text{feedstock}} \quad (12)$$

Finally, the weight loss (WL) of WT + Beta is represented as follows:

$$\text{WL} (\%) = 100 - Y_{\text{solid}} \quad (13)$$

2.6. Experimental apparatus and procedure

Wet torrefaction of wood cellulose pulp residue (WT WCPR) reactions were conducted in autoclave steel batch reactors (6 Parr 5000 Multiple Reactor System), each with a capacity of 75 mL and equipped with online pressure and temperature control regulators (Figs. S1–S3). Each vessel features an internal diameter of 1.50 inches, inner depths of 2.69 inches (with flat gasket) and 2.50 inches (with O-ring), a weight of 6 pounds (with head-mounted valves), and can withstand maximum temperature and pressure ratings of 300 °C and 200 bar, respectively. The reaction mixture was stirred using a magnetic stirring bar rotating at 800 rpm. Exactly 3.0 g of WCPR were introduced into each reactor vessel. In the case of the heterogeneously catalyzed reaction, 0.5–1.5 g of H-Beta zeolite with a SiO₂/Al₂O₃ ratio of 28 was added to the reactor vessels.

The electric heating temperature was meticulously controlled by the temperature program system, and the temperature inside the reactor was accurately monitored by an inline thermocouple. The initial reaction time began when the desired reaction temperature was achieved. The experiments considered five different torrefaction temperatures: 180, 200, 220, 240, and 260 °C, representing various levels of torrefaction from light to severe. Additionally, different durations of 15, 30, and 60 min, along with a fixed water/cellulose ratio of 10, were taken into account. In the present study, the water-to-WCPR ratio was chosen as 10, a selection based on the earlier research that involved optimizing the water amount for wet torrefaction of WCPR. After the reaction, the autoclave was rapidly cooled in an ice bath. The solid catalyst and the product solution were separated through filtration, and the product solutions were collected using a 0.22 μm membrane filter. Following separation, the hydrochars collected were dried overnight at 105 °C.

The collected liquid products underwent offline analysis employing a gas chromatography-mass spectrometry system, specifically, an Agilent GC-7890A coupled with an Agilent 5977B GC/MSD. This system was equipped with a DB-WAX Ultra Inert capillary column measuring 30 m in length, with an internal diameter of 0.25 mm and a film thickness of 0.25 μm. To identify and quantify these liquid products, an external calibration method was employed. It's worth noting that the standard deviations of liquid product distribution were found to fall within the range of ±4%, based on a minimum of three experimental repetitions.

3. Results and discussion

3.1. Effect of reaction time and temperature on the product distribution in the liquid phase of WT + Beta samples

Wet torrefaction, a hydrothermal treatment process conducted under moderate to elevated temperatures in the presence of water, has gained

significant attention as a promising pretreatment method for lignocellulosic biomass. The aim of wet torrefaction is to improve the biomass/biomass waste suitability for various downstream applications, including biofuel production, biorefining, and chemical synthesis. Understanding how key process parameters, such as reaction time, temperature, and catalyst loading influence the chemical composition of the resulting product is essential for optimizing this pretreatment technique.

The obtained data presents the results of a study investigating the effect of reaction time and temperature on the WT of WCPR with the addition of H-Beta zeolite catalyst (Fig. 1). The focus of the study appears to be on the product distribution in the liquid phase, specifically the conversion of cellulose into various chemical compounds such as levulinic acid, 5-HMF, furfural, acetic acid, methanol, and formic acid, in the presence of different reaction conditions. The typical GC-MS spectra of liquid products after WT of WCPR in the presence of H-Beta zeolite catalyst are presented in Fig. S4. The data indicates that the formation of furfural and 5-HMF generally decreases with increasing reaction time. This suggests that these compounds are likely intermediates or early products in the torrefaction process, which further undergo transformations to other compounds as the reaction progresses. After 60 min, furfural and 5-HMF levels have decreased significantly.

Acetic acid production shows some variation with reaction time. It increases at first but then stabilizes or decreases after 30 min. This indicates that acetic acid may be an intermediate product that is converted

into other compounds as the reaction proceeds. The production of methanol appears to decrease as the reaction time increases. This could be due to the conversion of methanol into other compounds. Levulinic acid production increases significantly with reaction time, indicating its formation as the reaction progresses. Formic acid also shows an increase, but its behavior is less clear and varies with other factors such as temperature. Ethanol production varies significantly with reaction temperature. It is notably high at 200 °C and 240 °C after 15 min but decreases at other temperatures. This suggests that ethanol formation is sensitive to temperature and likely peaks within a certain range.

Levulinic acid production appears to be highly temperature-dependent. It increases with temperature up to 220–260 °C. This suggests an optimal temperature range for levulinic acid production. Formic acid production also shows sensitivity to temperature. It is highest at 240 °C after 15 min and increases with temperature for longer reaction times.

The addition of H-Beta zeolite as a catalyst has a significant impact on the product distribution. It appears to enhance the formation of certain products, such as levulinic acid, while reducing others, such as furfural and 5-HMF. The catalyst likely promotes specific reaction pathways, influencing the selectivity of product formation. In summary, the data suggests that reaction time, temperature, and the presence of an H-Beta zeolite catalyst all play crucial roles in determining the product distribution in the wet torrefaction of wood cellulose pulp residue.

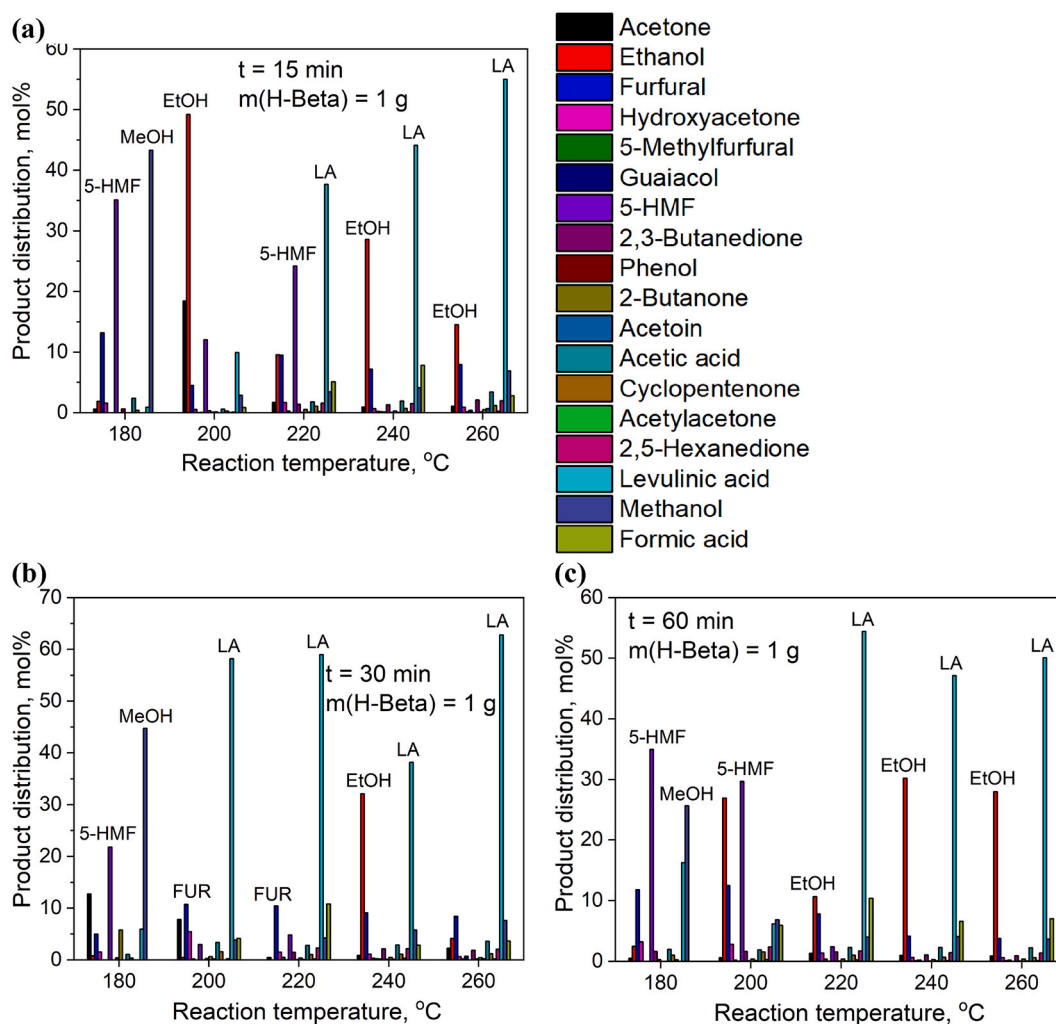


Fig. 1. Effect of reaction time (a – 15 min, b – 30 min, c – 60 min) and temperature on liquid-phase product distribution for the WT + Beta samples. Reaction conditions: 3.0 g of WCPR, 30 mL of water, 1.0 g of H-Beta catalyst, stirring speed at 900 rpm, reaction temperature ranging from 180 to 260 °C, and a reaction time of 15–60 min.

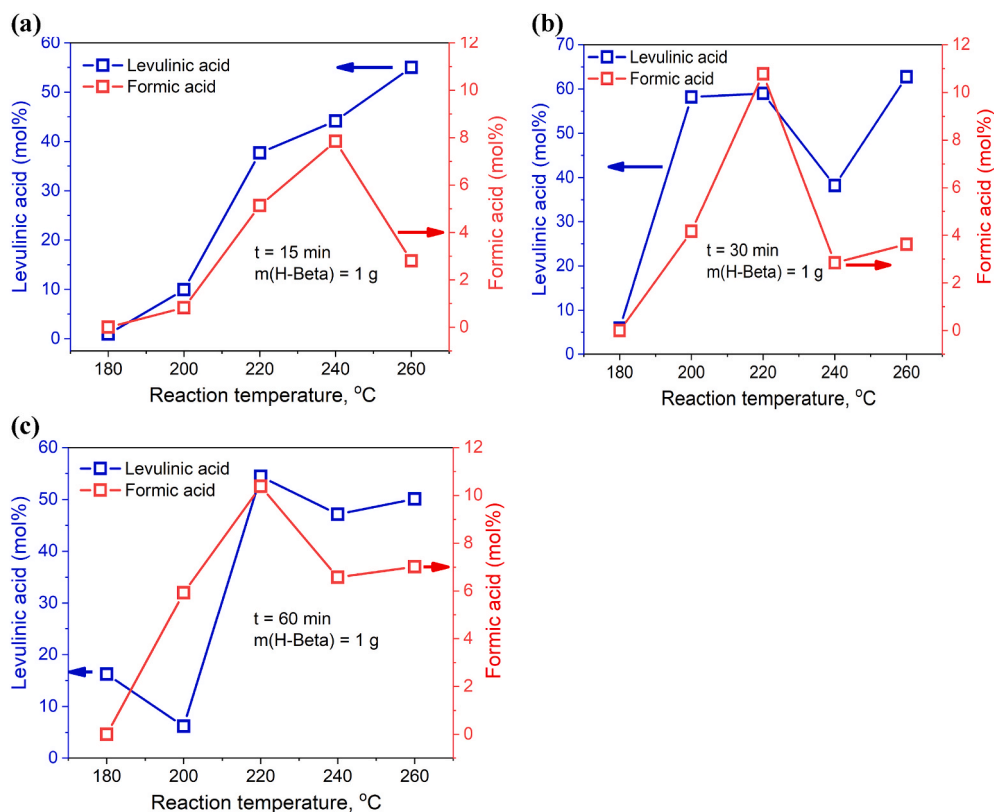


Fig. 2. Effect of reaction time (a – 15 min, b – 30 min, c – 60 min) and temperature on the amount of levulinic and formic acids for the WT + Beta samples. Reaction conditions: 3.0 g of WCPR, 30 mL of water, 1.0 g of H-Beta catalyst, stirring speed at 900 rpm, reaction temperature ranging from 180 to 260 °C, and a reaction time of 15–60 min.

The impact of reaction time and temperature on the levels of levulinic and formic acids in WT + Beta samples was investigated and is illustrated in Fig. 2. For both levulinic acid and formic acid production, there is a noticeable increase as the reaction time is extended from 15 to 30 min. This suggests that the torrefaction process is not complete within the initial 15 min and that longer reaction times are necessary for the conversion of cellulose/WCPR to these acids. Interestingly, the increase in levulinic acid production between 15 and 30 min is particularly pronounced at 220 and 260 °C, indicating that these temperatures are conducive to further conversion of cellulose into levulinic acid with extended reaction times. In contrast, formic acid production shows a more uniform increase across the temperature range from 15 to 30 min.

When comparing the data at 30 and 60 min, it's evident that levulinic acid production continues to increase with time at all temperatures, although the rate of increase slows down, especially at 260 °C. In contrast, formic acid production exhibits varying trends at different temperatures. At 220 °C, formic acid production increases significantly, but at 240 and 260 °C, it shows a decrease from 30 to 60 min, suggesting that at these higher temperatures, formic acid may undergo further reactions to produce other compounds. The impact of reaction temperature on levulinic acid production is significant. At 220–260 °C, there is a substantial increase in levulinic acid production compared to lower temperatures. This highlights the temperature sensitivity of the torrefaction process and suggests that higher temperatures favour the formation of levulinic acid.

In contrast, formic acid production shows a more complex relationship with temperature. It peaks at 220 °C after 30 min but decreases at 240 and 260 °C. This suggests that there is an optimal temperature range for formic acid production, and exceeding this range leads to the conversion of formic acid into other products. The addition of the H-Beta zeolite catalyst significantly enhances the production of both levulinic acid and formic acid compared to the non-catalyzed reaction. This

enhancement is particularly pronounced at higher temperatures and longer reaction times.

At 220 °C, the presence of the catalyst leads to a remarkable increase in both levulinic and formic acid production at 30 and 60 min. This indicates that the catalyst promotes the conversion of cellulose to these acids, especially at this temperature. At 260 °C, the catalyst's influence on formic acid production is more pronounced at 30 min but less so at 60 min, suggesting that the catalyst may facilitate formic acid formation in the early stages of the reaction, but its impact diminishes with extended reaction times. At a temperature of 220 °C, the H-Beta catalyst notably amplifies the production of levulinic acid within a mere 30 min, achieving an impressive peak selectivity of 58.9%, whereas at 260 °C, the highest selectivity attained was approximately 62.8%.

In conclusion, the data demonstrates that reaction time, temperature, and the addition of the H-Beta catalyst are critical factors in controlling the production of levulinic acid and formic acid during wet torrefaction. Optimization of these parameters is essential for tailoring the process to yield desired products efficiently, with potential applications in biofuel and chemical industries. Further studies may delve into the mechanistic aspects of these reactions to fully understand the underlying pathways and maximize the selectivity of product formation.

3.2. Effect of H-Beta catalyst loading on the product distribution in the liquid phase of WT WCPR

The presented study investigates the influence of H-Beta zeolite catalyst loading on the wet torrefaction process of WCPR (Fig. 3a and b). The results show a clear trend in the production of levulinic acid with varying catalyst loadings. As the catalyst loading increased from 0.5 g to 1.0 g, the selectivity of levulinic acid increased significantly from 46.1 to 59.0%. This initial increase can be attributed to the enhanced catalytic activity of H-Beta zeolite, facilitating the conversion of WCPR to

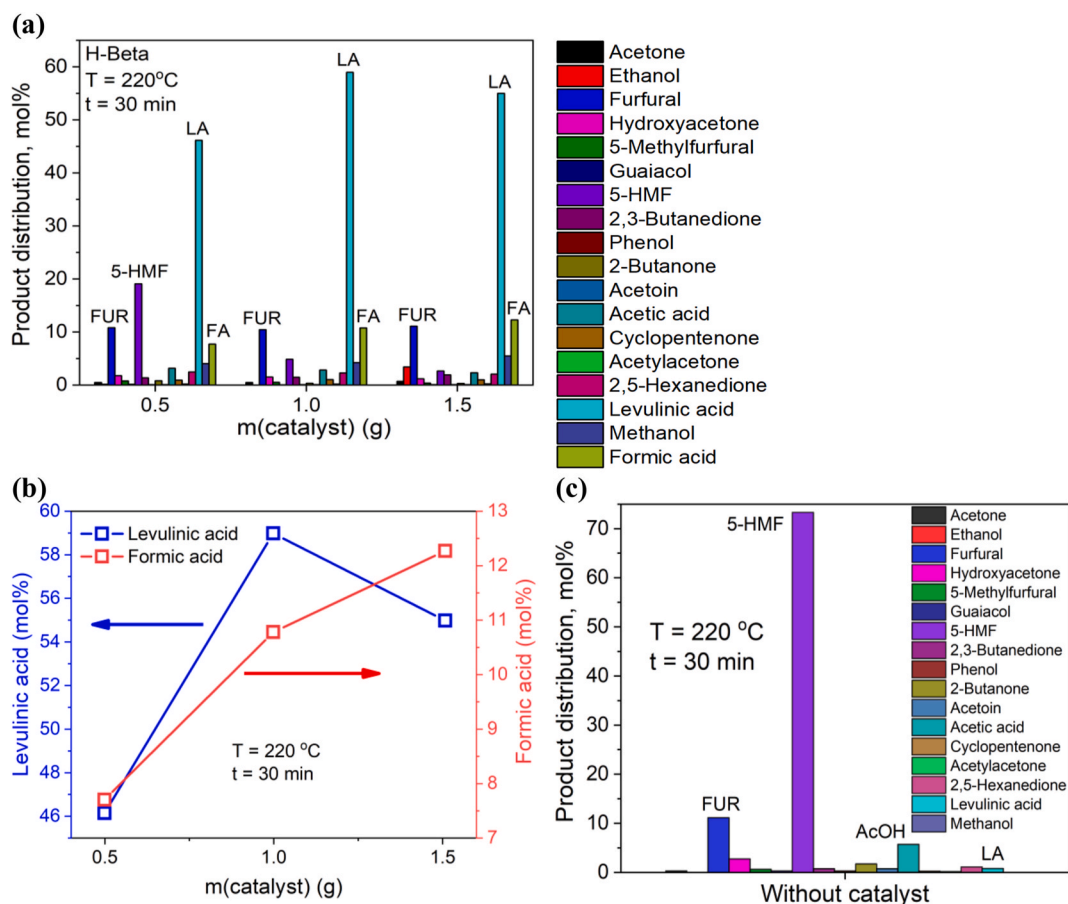


Fig. 3. (a, b) – effect of catalyst loading on liquid-phase product distribution in WT + Beta; (c) – the product distribution without presence of catalyst. Reaction conditions: 3.0 g of WCPR, 30 mL of water, 0–1.5 g of H-Beta catalyst, stirring speed at 900 rpm, reaction temperature at 220 °C, and a reaction time of 30 min.

levulinic acid. However, the subsequent decrease in levulinic acid selectivity observed when the catalyst loading was further increased to 1.5 g is intriguing. It suggests that beyond a certain threshold, excess catalyst may lead to side reactions, impacting levulinic acid production.

The study also reports a similar trend in formic acid production. The formic acid selectivity increased from 46 to 58% as the catalyst loading increased from 0.5 to 1.5 g. This increase could be attributed to the catalytic role of H-Beta zeolite in promoting the conversion of WCPR to formic acid. However, the specific mechanisms underlying this effect need to be elucidated. Understanding the catalyst's role in the formation of different organic acids is essential for optimizing the wet torrefaction process.

Interestingly, the study finds that the production of furfural remains relatively consistent across different catalyst loadings, ranging from 10.8% to 11.1%. This stability in furfural selectivity suggests that the H-Beta zeolite catalyst may not significantly impact furfural formation in the wet torrefaction process. On the other hand, 5-HMF production exhibits a significant decrease from 19.1 to 2.6% as the catalyst loading increases. This decline could be due to the catalyst's role in promoting the conversion of 5-HMF via rehydration to other products such as levulinic and formic acids. The results indicate that there is an optimal catalyst loading (1.0 g) for maximizing the production of target compounds like levulinic acid. Beyond this amount, diminishing returns or adverse effects on selectivity may occur.

In Fig. 3c, it is evident that in the absence of a catalyst during WT WCPR under identical reaction conditions, the primary reaction product was 5-HMF, exhibiting a selectivity exceeding 70%. This observation highlights that the introduction of a catalyst with acid sites facilitates the conversion of 5-HMF into levulinic acid and formic acid. This

transformative process has been experimentally validated and is further elucidated in the discussion accompanying the reaction mechanism presented in Fig. 10.

Moreover, the results presented in Tables 2 and 3 demonstrate the significant impact of the H-Beta catalyst under identical reaction conditions ($T = 220\text{ °C}$, $t = 30\text{ min}$, $\text{H}_2\text{O}/\text{WCPR} = 10$). The presence of the H-Beta catalyst resulted in notable improvements across various parameters. Specifically, HHVs increased from 20.6 to 30.3 MJ/kg, reflecting enhanced energy content. Carbon content witnessed a substantial rise, escalating from 51.6 to 78.9 wt%, with fixed carbon content also exhibiting an increase from 21.7 to 28.1 wt%. Furthermore, the enhancement factor experienced a notable elevation from 1.07 to 1.51, indicating a more efficient reaction. Carbon enrichment showed a significant rise, from 1.07 to 1.63, emphasizing the catalyst's positive influence on carbon-based products. The BET surface area expanded significantly from 2.7 to 29.1 m^2/g , suggesting improved structural characteristics. Simultaneously, there was a substantial increase in weight loss, from 26.5 to 60.7%, underlining the catalyst's impact on the decomposition process. Concurrently, the amount of oxygen decreased sharply from 39.9 to 12.0 wt%, indicating a reduction in oxygenated compounds. The O/C ratio also declined from 0.6 to 0.1, reflecting a shift towards a more carbon-rich composition. These comprehensive findings underscore the favorable influence of the H-Beta catalyst on the specified reaction parameters, highlighting its role in enhancing both energy content and structural characteristics of the resulting products.

3.3. TG analysis of WCPR and WT + Beta samples

The thermogravimetric analysis (TG) conducted on both WCPR and

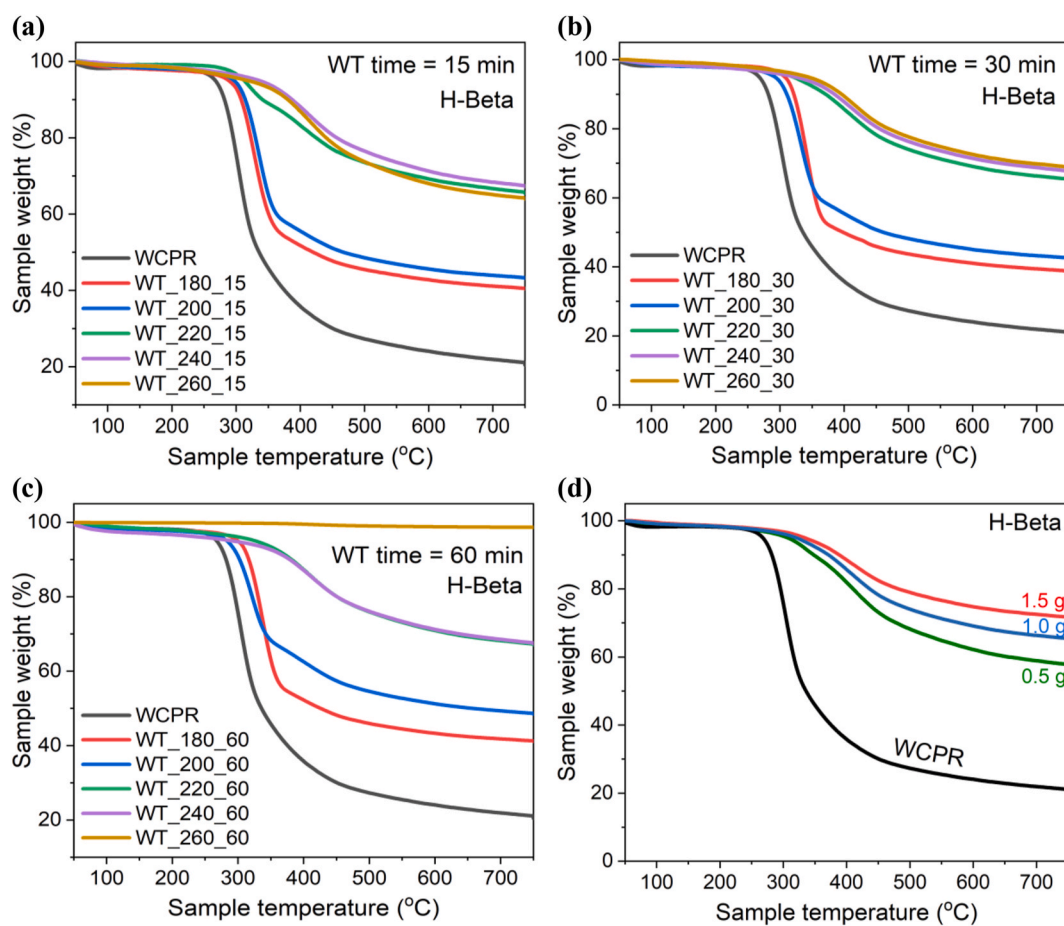


Fig. 4. TG curves of WCPR and WT WCPR material with 1 g of H-Beta catalyst at 15 min – (a), 30 min – (b) and 60 min – (c) in the temperature range of 50–750 °C – (a) and with different amount of catalyst loading – (d) at the heating rate of 10 °C/min in nitrogen atmosphere.

wet torrefied WCPR samples has yielded valuable insights into their pyrolysis behavior under various temperature conditions in a nitrogen atmosphere (Fig. 4). These insights contribute significantly to a deeper understanding of the thermal stability and decomposition characteristics inherent in these materials. To investigate the pyrolysis behavior, a temperature range spanning from 50 to 750 °C was selected.

One notable observation from the TG analysis is that the most substantial weight loss for samples such as dry cellulose (WCPR), WT₁₈₀, and WT₂₀₀ occurs after crossing the 250 °C threshold, whereas for WT₂₂₀, WT₂₄₀, and WT₂₆₀ samples, this pivotal transition point is seen after surpassing 350 °C. This temperature transition is a crucial juncture in the thermal decomposition and stability of these materials.

Furthermore, the TG analysis unveiled that WCPR exhibited the highest weight loss within the temperature range of 275–350 °C. Wet torrefaction is known to influence the thermal characteristics of biomass-derived materials. The study highlights how different torrefaction temperatures impact pyrolysis behavior. Notably, samples subjected to higher torrefaction temperatures exhibited greater thermal stability and more significant reductions in weight loss compared to other torrefaction conditions. This observation suggests that high-temperature torrefaction enhances the material's thermal stability, potentially by eliminating volatile components and inducing structural changes.

The wet torrefied sample at 260 °C exhibited the highest thermal stability, indicating a unique influence of wet torrefaction on the pyrolysis process at later stages (Fig. 4c). Remarkably, the sample subjected to torrefaction at 220 °C not only demonstrated exceptional thermal stability but also exhibited the most favorable liquid product distribution across the entire temperature range assessed. This

observation strongly suggests that torrefaction at this particular temperature setting imparts outstanding thermal resilience to the material while simultaneously promoting the formation of valuable liquid products within the parameters of the study. In the TG curves (Fig. 4c), there is a notable increase in residual mass, which escalates from 21.2% (WCPR) to 98.7% (WT_{260_60}) as the WT temperature rises. This trend is attributed to a larger proportion of mass in WCPR being lost during the WT process at higher temperatures (Zhu et al., 2022). Importantly, the residual masses of WT_{180_30} (38.8%), WT_{200_30} (42.8%), WT_{220_30} (65.3%), WT_{240_30} (67.8%), and WT_{260_30} (68.9%) samples were 1.83, 2.02, 3.08, 3.20, and 3.25 times higher, respectively, than that of the WCPR raw material (21.2%) (Fig. 4b). This observation suggests an enhancement in thermal stability with increasing WT pre-treatment temperatures. Additionally, the effect of catalyst loading on thermal stability was explored, employing three different loadings of H-Beta zeolite catalyst: 0.5, 1.0, and 1.5 g. The findings revealed (Fig. 4d) that the wet torrefied sample with 1.5 g of H-Beta catalyst exhibited the highest thermal stability.

3.4. HR SEM analysis of WCPR and WT + Beta samples

The SEM scan images presented in Fig. 5 demonstrate significant differences between the dried cellulose sample and the sample subjected to the most optimal reaction conditions ($T = 220$ °C, $t = 30$ min, water/WCPR = 10) with the use of H-Beta zeolite catalyst for wet torrefaction. The dried cellulose exhibits a relatively porous structure, which is characteristic of untreated biomass materials. However, after undergoing wet torrefaction, the cellulose surface undergoes a transformative process, adopting a flat and smoother texture. This remarkable change in

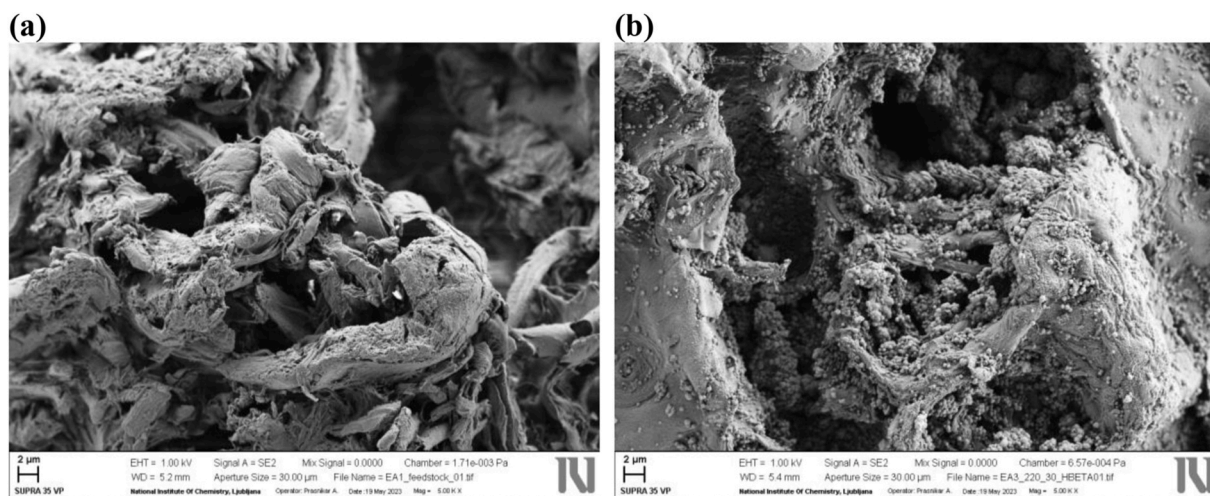


Fig. 5. SEM scans of WCPR – (a) and WT + Beta samples at 220 °C after 30 min – (b).

morphology can be attributed to the thermochemical reactions that take place during the wet torrefaction process. One of the key indicators of successful wet torrefaction under the optimized conditions is the observed increase in levulinic acid content in the liquid product. The H-Beta zeolite catalyst plays a crucial role in facilitating the wet torrefaction process, likely by promoting the formation of intermediates and selectively catalyzing specific reactions leading to the production of levulinic acid and other valuable products. The acidic and porous nature of the H-Beta zeolite provides an ideal environment for catalytic reactions to occur, allowing for the effective conversion of cellulose into valuable chemicals.

The SEM-EDX analysis provides valuable information about the elemental composition of the cellulose feedstock and the changes that occur after wet torrefaction with the H-Beta catalyst. The carbon content in the cellulose decreases significantly from approximately 58% in the feedstock to around 46% in the wet torrefied sample (Table 1). This reduction in carbon content indicates the conversion of cellulose into other products, such as levulinic acid and other degradation byproducts, during the wet torrefaction process. Correspondingly, the oxygen content increases, which is consistent with the production of oxygen-containing compounds during the torrefaction.

Silicon is detected in trace amounts in the WCPR feedstock, and its presence is more pronounced in the wet torrefied sample (WT + Beta_220), along with the appearance of aluminium (Fig. S5). These elements could be attributed to the introduction of the H-Beta catalyst during the torrefaction process. The sulfur content in both the feedstock

Table 1
SEM-EDX analysis of the WCPR and WT + Beta samples at 220 °C for 30 min.

WCPR			
Element	Scan 1 (wt%)	Scan 2 (wt%)	Scan 3 (wt%)
C	57.97	58.57	57.97
O	41.69	41.27	41.85
Si	0.06	–	0.06
Al	–	–	–
S	0.14	–	–
Ca	0.13	–	0.13
Fe	–	–	–
WT + Beta_220			
C	45.57	45.15	46.57
O	45.45	44.76	43.72
Si	8.23	8.81	8.90
Al	0.69	0.71	0.73
N	–	0.56	–
Ca	0.06	–	0.08

and wet torrefied sample is relatively low, with some variation between scans.

Calcium is detected in trace amounts in the feedstock and remains at low levels in the wet torrefied sample. These elements might originate from impurities in the biomass or catalyst. Iron is not detected in the feedstock but appears in minimal quantities in one of the scans of the wet torrefied sample. As with other trace elements, the presence of iron might be attributed to impurities in the biomass.

3.5. XRD analysis of WCPR and WT + Beta samples

The X-ray diffraction (XRD) patterns obtained for both the wood cellulose pulp residue and the corresponding wet torrefied samples (Fig. 6) displayed notable peaks at 2θ values of 15.6°, 22.4°, and 34.4°.

These specific peaks were attributed to the crystalline planes indexed as (110), (200), and (004), respectively, within the crystal structure of the cellulose type I allomorph. It is crucial to emphasize that cellulose is the sole component characterized by a crystalline structure, while hemicellulose and lignin exhibit amorphous characteristics (Li et al., 2015). These results highlight the transformation in the crystalline integrity of cellulose during the wet torrefaction process, indicating a reduced polymorphic structure of cellulose I within the temperature range of 180–200 °C. However, in samples subjected to wet torrefaction at temperatures between 220 and 260 °C, a distinct disappearance of characteristic cellulose peaks was notably observed. At the same time, it was detected the XRD pattern of the H-Beta zeolite catalyst related to BEA topology (JCPDS No. 47–0183) with high crystallinity and the strong intensity diffraction peaks observed in 2θ region of 5–25° at 7.8, 13.4, 14.6, 21.5, 22.5° (Kostyniuk et al., 2021b).

3.6. Elemental components and surface properties of WCPR and WT + Beta samples

In Table 2, a comprehensive examination of the proximate and elemental composition, surface area, and pore diameter of both WCPR and WT + Beta samples is provided. These examinations were conducted over a temperature range of 180–260 °C, each lasting 30 min. The preference for the 30 min torrefaction period stems from its optimal suitability when compared to both 15 and 60 min. The decision to select a 30 min WT time is influenced by its impact on the distribution of liquid products (Fig. 1b) and the enhancement of the resulting hydrochar's quality (Fig. 4b).

The proximate analysis, which includes moisture, volatile matter (VM), fixed carbon (FC), and ash, demonstrates a significant change in the composition of the feedstock as a result of wet torrefaction. As shown

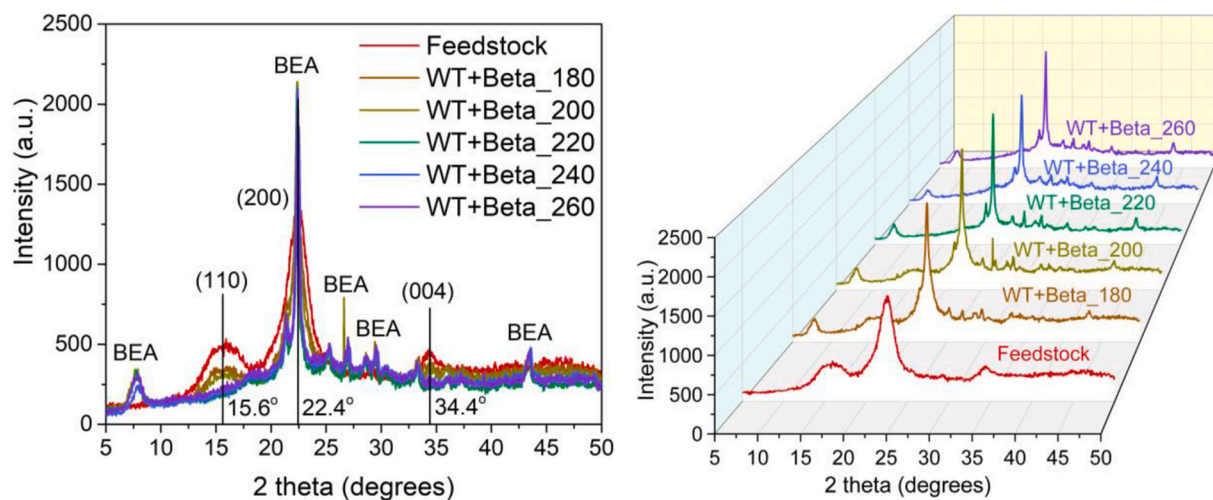


Fig. 6. X-ray diffraction pattern of the WT WCPR samples with H-Beta catalyst at 180–260 °C (“WT + Beta_180”–“WT + Beta_260”) as compared to the WCPR (“feedstock”).

in Table 2, at higher WT temperatures, such as 220–260 °C, the moisture content decreases to around 2–4%. The fixed carbon content is a critical parameter influencing the heating value and combustion properties of a material. The data reveals a notable change in fixed carbon content as a result of wet torrefaction at different temperatures. WT_220 and WT_260 samples exhibit significantly higher fixed carbon content compared to the initial WCPR. Specifically, at 220 °C, fixed carbon content increases to 28.1%, and at 260 °C, it reaches 31.3%. This transformation indicates that wet torrefaction effectively removes volatile components and non-carbonaceous matter from the feedstock. Also it was observed a substantial reduction in volatile matter content with increasing torrefaction temperature. The initial WCPR has a volatile matter content of 75.5%, which decreases significantly after wet torrefaction. For instance, at 220 °C, the volatile matter content reduces to 28.6%, and at 260 °C, it further decreases to 29.0%. In direct comparison to coal, biomass fuel exhibits a significant drawback, characterized by its elevated volatile matter and reduced fixed carbon content. However, the incorporation of WT proves to be a valuable solution to address these concerns. WT works to reduce VM and elevate FC in the hydrochar, thereby transforming the fuel into a product that shares more closely related characteristics with coal, as substantiated in reference (Bach and Skreiberg, 2016).

In addition, it was found that the initial WCPR has an ash content of 3.2%, which significantly increases after wet torrefaction. For example, at 220 °C, the ash content rises to 41.1%, and at 260 °C, it further increases to 37.1%. The significant increase in ash content can be attributed to the addition of H-Beta zeolite catalyst during the wet torrefaction process. This catalyst includes SiO₂ and Al₂O₃, which remain relatively stable even at the elevated temperatures.

The CHN(O)S elemental analysis is a comprehensive method used to determine the C, H, O, N and S content in samples (Table 2 and Fig. 9b). Carbon content, a critical parameter for assessing fuel and biomass materials, provides insights into the proportion of carbonaceous material within the sample. Notably, as the severity of WT increases, there is a distinct and consistent trend of rising carbon content. The untreated WCPR sample contains 48.3% carbon, whereas the carbon content significantly increases to 78.9% in the WT + Beta_220 sample. This notable increase signifies WT’s effectiveness in concentrating carbon, thereby enhancing the resulting hydrochar’s carbon richness and potential suitability as a fuel source.

Concurrently, the analysis of oxygen content is pivotal due to its direct influence on combustibility and energy content. As WT severity escalates, a conspicuous reduction in oxygen content becomes apparent. The untreated WCPR sample features 40.3% oxygen, whereas the WT +

Beta_220 sample exhibits a notably reduced oxygen content of 12.0%. This decrease underscores the WT process’s ability to diminish oxygen-rich functional groups in the biomass, an advantageous alteration that contributes to improved fuel characteristics. The hydrogen content also exhibited a notable decrease in the WT + Beta samples in comparison to the WCPR feedstock, decreasing from 6.2% to 3.2%. In contrast, N and S contents remain relatively stable across all the samples studied. While minor fluctuations are observed, these variations remain within a narrow range and are not expected to have a significant impact on the properties of the WT samples.

The specific surface area, as determined by the BET method (presented in Table 2), displays notable variations in response to the severity of wet torrefaction (WT) treatment. During the initial stages of WT (e.g., WT + Beta_180 and WT + Beta_200), there are significant increases in surface area (106.3 and 97.5 m²/g, respectively) compared to the untreated WCPR (3.4 m²/g). This enhancement can be attributed to the incorporation of Beta zeolite, known for its high surface area. However, as WT severity decreases, there is a substantial reduction in surface area, declining from 106.3 to 8.9 m²/g. This observation indicates that heightened torrefaction severity leads to a reduction in surface area, potentially attributed to the release of specific reaction products and structural modifications within the WCPR.

Conversely, the average pore diameter (PD), evaluated through the BJH method, shows a decrease as WT severity increases. In the early stages of WT (e.g., WT + Beta_180 and WT + Beta_200), there is a significant decrease in pore diameter (measuring 60.3 and 70.9 Å, respectively) in comparison to the untreated WCPR (393.7 Å). This suggests that initial torrefaction stages lead to the expansion of the pore network. However, with increased WT severity, there is a notable increase in pore diameter, particularly in the WT + Beta_220 sample, featuring a pore diameter of 196.5 Å, and the WT + Beta_260 sample, which exhibits a pore diameter of 173.2 Å. This observation suggests that as torrefaction severity intensifies, there is an expansion in the size of the pores, potentially attributed to the more thorough removal of volatile components and the formation of a more porous structure, as well as structural alterations within the WCPR. These findings align with the results obtained from morphological, structural, and thermal analyses, as well as the study on the distribution of liquid products.

3.7. HHV, solid, carbon, hydrogen, energy yields, DC, DH, DO, enhancement factor, carbon enrichment, weight loss and atomic ratios of O/C and H/C of WCPR and WT + Beta samples

This study presents a thorough investigation into the higher heating

Table 2

Proximate and elemental analysis, BET surface area and pore diameter (PD) of the WT + Beta samples as compared to the WCPR.

Samples	T, °C	t, min	H ₂ O/WCPR ratio	Proximate analysis (wt%)				Elemental analysis (wt%)						BET surface area, m ² /g	PD ^c , Å
				Moisture	VM ^a	FC ^b	Ash + Si + Al	C	H	O	N	S	Si + Al		
WCPR	–	–	–	1.5	75.5	19.8	3.2	48.3	6.2	40.3	0.1	0.5	0	3.4	393.7
WT + Beta_180	180	30	10	3.0	57.2	15.6	24.2	57.9	5.0	30.8	0.1	0.1	6.1	106.3	60.3
WT + Beta_200	200	30	10	7.6	48.7	17.7	26.0	60.4	4.7	23.7	0.1	0.2	10.9	97.5	70.9
WT + Beta_220	220	30	10	2.3	28.6	28.1	41.1	78.9	3.4	12.0	0.1	0.1	5.5	29.1	196.5
WT + Beta_240	240	30	10	3.8	29.1	31.2	35.9	74.0	3.3	15.4	0.1	0.1	7.1	49.3	128.7
WT + Beta_260	260	30	10	2.6	29.0	31.3	37.1	74.7	3.2	16.1	0.1	0.1	5.8	8.9	173.2
WT_WCPR_220 ^d	220	30	10	1.2	76.2	21.7	1.0	51.6	6.1	39.9	0.1	0.1	0	2.7	369.1

^a VM – volatile matter.^b FC – fixed carbon.^c PD – Average pore diameter measured from the desorption branch according to the BJH method.^d WT_WCPR_220 – wet torrefaction of wood cellulose pulp residue without presence of catalyst.

values (HHVs) of untreated WCPR and WT + Beta samples. The results of this analysis are meticulously tabulated in Table 3 and visually depicted in Fig. 7a. It's noteworthy that the HHVs of the WT + Beta samples, tested in a controlled environment using N₂, consistently increase as the temperature rises.

This increase ranges from 20.1 MJ/kg for untreated WCPR to an impressive 30.3 MJ/kg for the WT + Beta_220 sample. This rising HHV at 220 °C is a promising outcome of the WT process. In simple terms, this means that WT-treated biomass can be a much better quality and more energy-dense solid fuel compared to untreated WCPR. These findings are significant and suggest that WT in the presence of a zeolite catalyst is a robust method for improving the energy content and quality of bio-based fuels. At higher temperatures (240 and 260 °C), WCPR components undergo thermal decomposition reactions, leading to the release of volatile compounds and leaving behind a charred residue. This decomposition process can result in a decrease in the HHV as the original energy content of the WCPR is lost which is similar to the results obtained by Li et al. (2020).

Table 3 provides crucial data on solid yield, reflecting the proportion of solid material obtained after the WT treatment of WCPR. Notably, as the severity of the WT treatment escalates, there is a significant reduction in solid yield. The untreated WCPR sample, which serves as the reference point, does not have a specified value. However, the solid yield decreases from 83.0% (WT + Beta_180) to 39.7.9% (WT + Beta_260) under more rigorous treatment conditions. This decline in solid yield is attributed to the removal of volatile components and the conversion of biomass into a more carbon-rich, energy-dense form, thereby enhancing fuel quality.

Furthermore, the van Krevelen diagram, thoughtfully presented in Fig. 7b, depict weight profiles alongside atomic H/C and atomic O/C ratios. This diagram unveil a consistent linear pattern in which H/C and O/C ratios decrease with rising temperatures under an N₂ atmosphere. This aligns with observations from previous studies (Zhang et al., 2019). The decrease in H/C and O/C ratios observed in the van Krevelen diagram indicates a notable enhancement in carbonization (He et al., 2018). This reduction in ratios implies a refinement in the carbonization process with increasing temperatures, highlighting a significant correlation between temperature and the efficacy of carbonization.

Energy yield, as indicated in Table 3 and Fig. 7a, measure the efficiency of the WT process in preserving the energy content of the WCPR post-treatment. Notably, as the severity of WT treatment increases, the energy yield decreases. For instance, WT + Beta_180 sample maintain relatively high energy yields at 94.5%. However, with heightened severity (WT + Beta_260), the energy yield decreases to 55.6%. These results indicate that more intense WT conditions result in reduced energy yield, primarily due to the loss of volatile components and increased liquid product formation.

Table 3 also offers valuable insights into carbon yield, which signifies the percentage of carbon content obtained following WT treatment of

the WCPR, in comparison to the original untreated WCPR. The reference point is the untreated WCPR sample, which lacks a specified value. Carbon yield exhibits a decreasing trend as torrefaction severity intensifies, diminishing from 83.0% (WT + Beta_180) to 39.7% (WT + Beta_260) under the most rigorous treatment conditions. This reduction in carbon yield primarily stems from the removal of volatile components, decrease of solid yield, and the conversion of biomass into a more carbon-rich form during wet torrefaction (Chen et al., 2022; Wang et al., 2018).

Similar to carbon yield, the WCPR sample acts as the reference point for hydrogen yield and does not possess a specified value. Hydrogen yield also experiences a decrease as torrefaction severity increases, dropping from 66.4% (WT + Beta_180) to 20.3% (WT + Beta_260) under the most severe treatment conditions. The decline in hydrogen yield is attributed to the removal of hydrogen-rich volatile components during wet torrefaction. These findings underscore the influence of torrefaction severity on carbon and hydrogen yield, with more severe torrefaction conditions leading to a reduction in both, emphasizing the transformation of biomass into a more carbon-rich and energy-dense form. This dataset holds significant value in comprehending the compositional changes during WT and its implications for biomass conversion processes.

The enhancement factor, a ratio indicating the improvement in energy yield through WT treatment of WCPR, consistently exceeds 1.0 for all WT + Beta samples. This underscores that the WT process enhances energy yield in comparison to untreated WCPR (Table 3). The enhancement factor increases as torrefaction severity rises, ranging from 1.14 (WT + Beta_180) to 1.51 (WT + Beta_220), signifying that more intense treatment conditions result in a greater enhancement of energy yield.

In Fig. 8, the profiles of enhancement factors are displayed against the atomic O/C ratio and carbon enrichment for both WCPR and WT + Beta samples. Notably, both correlations exhibit a good linear trend as carbon enrichment or atomic O/C ratio increases. An increase in carbon enrichment leads to a higher enhancement factor, while an increase in the O/C ratio corresponds to a lower enhancement factor.

Table 3 and Fig. 9 provide data on decarbonization (DC), dehydrogenation (DH), and deoxygenation (DO) for various samples and elemental analysis, including untreated WCPR and WT + Beta samples at different reaction temperatures. The element removal sequence during torrefaction, where DO > DH > DC, highlights torrefaction's pronounced effect on reducing oxygen content compared to other elements (Chen et al., 2022). Decarbonization measures the reduction in carbon content in the biomass during the WT process, with the data revealing a gradual increase in DC with rising treatment severity. For instance, DC rate in the WT + Beta_180 (0.6%) sample is low but experience a significant increase in the WT + Beta_200 (45.0%). A similar pattern is notably present in DH and DO, but the increase is much more pronounced, reaching 67.9% and 82.4%, respectively. This consistent trend

Table 3
HHV, solid yield, carbon yield, hydrogen yield, energy yield, DC, DH, DO, enhancement factor, atomic ratios, CE and WL of the WT + Beta samples as compared to the WCPR.

Samples	T, °C	t, min	H ₂ O/WCPR ratio	HHV, MJ/kg	Solid yield, wt %	Carbon yield, wt %	Hydrogen yield, wt %	Energy yield, %	DC ^a , %	DH ^b , %	DO ^c , %	Enhancement factor	Atomic ratio		
													O/C	H/C	CE ^d , %
WCPR	–	–	–	20.1	–	–	–	–	–	–	–	1.00	0.6	1.5	1.00
WT + Beta_180	180	30	10	22.9	83.0	99.4	66.4	94.5	0.6	24.4	27.9	1.14	0.4	1.0	1.20
WT + Beta_200	200	30	10	24.2	44.0	55.0	33.5	53.0	45.0	59.6	68.8	1.21	0.3	0.9	1.25
WT + Beta_220	220	30	10	30.3	39.3	64.2	21.3	59.2	35.8	67.9	82.4	1.51	0.1	0.5	1.63
WT + Beta_240	240	30	10	28.2	43.4	66.5	23.2	60.8	33.5	67.5	76.7	1.40	0.2	0.5	1.53
WT + Beta_260	260	30	10	28.2	39.7	61.3	20.3	55.6	38.7	71.5	77.7	1.40	0.2	0.5	1.55
WT_WCPR_220 ^f	220	30	10	20.6	73.5	78.5	71.8	78.9	21.5	28.2	27.3	1.07	0.6	1.4	1.07

^a DC – decarbonization.

^b DH – dehydrogenation.

^c DO – deoxygenation.

^d CE – carbon enrichment.

^e WL – weight loss.

^f WT_WCPR_220 – wet torrefaction of wood cellulose pulp residue without presence of catalyst.

signifies that as the severity of WT conditions intensifies, there is a substantial removal of oxygen (O), hydrogen (H), and carbon (C) from the WCPR. This outcome holds significant importance as it contributes to a reduction in carbon content and enhances the C/H and C/O ratios in the resulting hydrochar. These transformations render the hydrochar more suitable as a solid fuel source, boasting improved fuel characteristics suitable for a range of applications. In conclusion, the investigation revealed (Table 3) that the weight loss (WL) of WCPR varied within the range of 17.0–60.7%, with the WT + Beta_220 sample displaying the highest WL. Notably, as the wet torrefaction temperature exceeded 180 °C, there was a substantial increase in WL, transitioning from 17.0 to 56.0%.

To enrich the discussion and facilitate comparison with the findings of other researchers, a thorough analysis of data was undertaken. The results are presented in Table S4, which compares the HHV and elemental composition of hydrochar derived from various types of biomass following wet torrefaction under optimal reaction conditions. Table S4 illustrates that the WT + Beta_220 sample exhibits the highest HHV (30.3 MJ/kg) and carbon content (78.9 wt%) in hydrochar compared to a range of biomass types documented in literature (Dai et al., 2017; Jian et al., 2019; Ma et al., 2018; Missaoui et al., 2017; Volpe and Fiori, 2017; Wang et al., 2018; Wang et al., 2018, 2018; Zhang et al., 2017). There is a consistent trend across all biomass types, showing an increase in HHV with temperature, with HHV strongly correlating with the carbon, hydrogen, oxygen, and nitrogen contents of the biomass. Despite the wet torrefaction temperature being the lowest (220 °C) compared to other studies, the HHV and carbon content surpass theirs in our study, while still maintaining the lowest oxygen content (12.0 wt%). The improvement in HHV (Fig. 7a) of wet torrefied WCPR is attributed to the higher concentration of carbon and reduced oxygen content (Fig. 7b). This results from more pronounced dehydration reactions facilitated by the presence of the H-Beta catalyst compared to biomass feedstock from literature where the catalyst was absent (Table S4). Additionally, it is proposed that the decrease in oxygen content primarily stems from the degradation of cellulose due to the reaction with the acidic H-Beta zeolite catalyst, considering its oxygen-rich nature relative to lignin. Therefore, the careful selection of the temperature range for wet torrefaction of lignocellulosic biomass is crucial, taking into account the diverse properties of different biomass sources to ensure efficient production and cost-effectiveness (Kostyniuk and Likozar, 2024). The findings carry significant implications for the practical production of high-quality hydrochar and levulinic acid products from biomass waste in the future, particularly with ongoing enhancements in catalyst efficiency, selectivity, and durability. The research addresses a critical gap in the literature by offering insights into the optimal conditions for wet torrefaction and the potential of the one-pot chemocatalytic approach for biomass valorization.

3.8. Reaction pathways of WCPR into hydrochar and the liquid products

The synthesis of levulinic acid from cellulose derived from lignocellulosic biomass necessitates a multistep process involving cellulose hydrolysis to glucose (Abdu et al., 2020), glucose conversion to 5-hydroxymethylfurfural (5-HMF), and subsequent transformation of 5-HMF into levulinic acid (Li et al., 2019). However, this procedure is challenged by several inherent complexities. Cellulose's tightly packed crystalline structure, replete with both inter- and intramolecular hydrogen bonding, presents a formidable obstacle. Furthermore, cellulose is insoluble in water and most common solvents, and its chemical stability remains resilient across a broad range of conditions.

In light of the acquired product distribution data and a thorough analysis of the existing literature, an extensive reaction network has been constructed aimed at providing a clear depiction of the transformation of cellulose (WCPR) into a diverse array of valuable chemical products. This transformation is achieved through WT WCPR catalyzed by an H-Beta zeolite catalyst, and it encompasses the production of

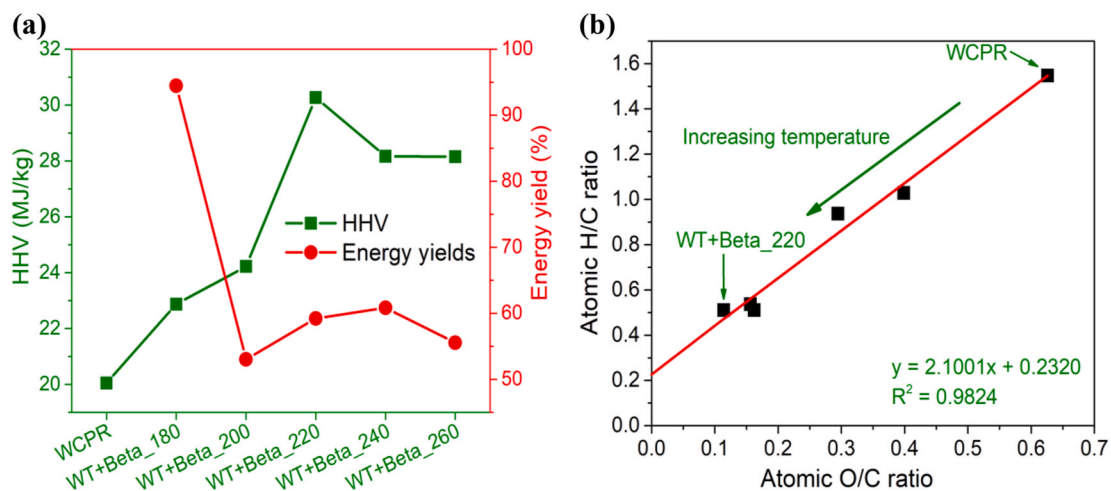


Fig. 7. HHV and energy yield – (a) and H/C versus O/C ratio in terms of atomic basis (van Krevelen diagram) – (b) for WCPR and WT + Beta samples.

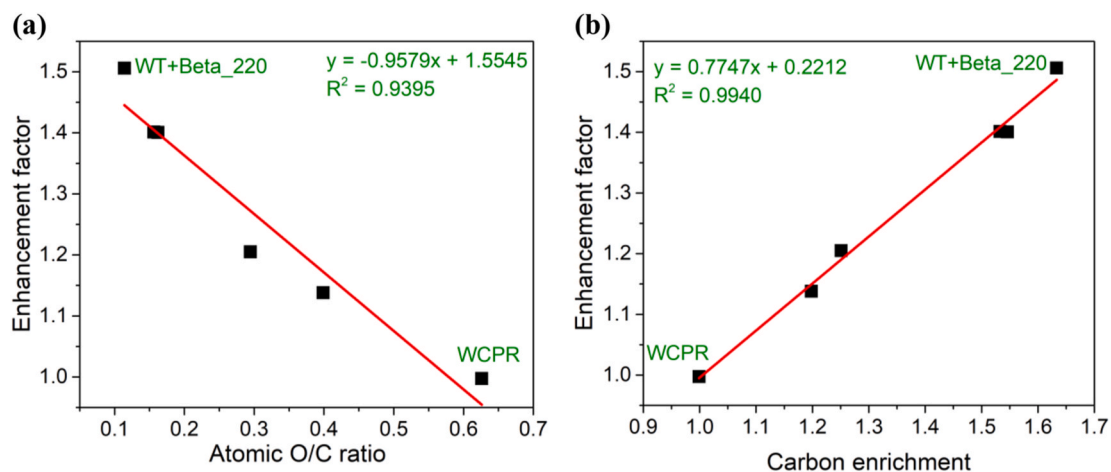


Fig. 8. Enhancement factor versus O/C ratio – (a) and carbon enrichment – (b) for WCPR and WT + Beta samples.

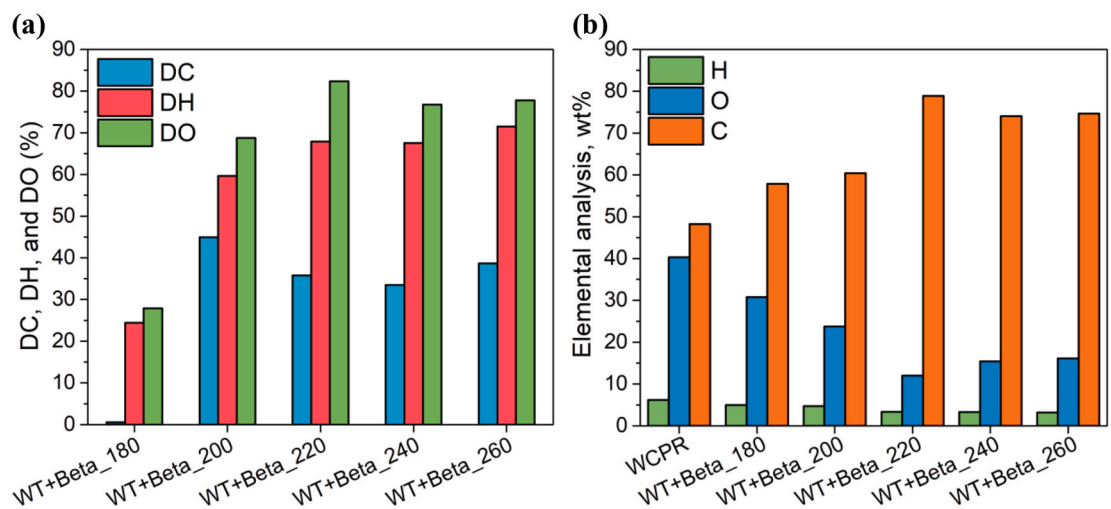


Fig. 9. (a) – profiles of decarbonization (DC), dehydrogenation (DH), and deoxygenation (DO) and (b) – elemental analysis (H, O, C) of WCPR and WT + Beta samples in the temperature range of 180–260 °C.

various compounds, prominently featuring levulinic acid, 5-HMF, hydroxyacetone, furfural, formic acid, acetaldehyde, ethanol, methanol, acetic acid, and others, as presented in Fig. 10.

The sequence for the conversion of cellulose into these valuable compounds involves several discrete steps. Initiation is marked by cellulose hydrolysis into glucose, catalyzed by the H-Beta zeolite's acid

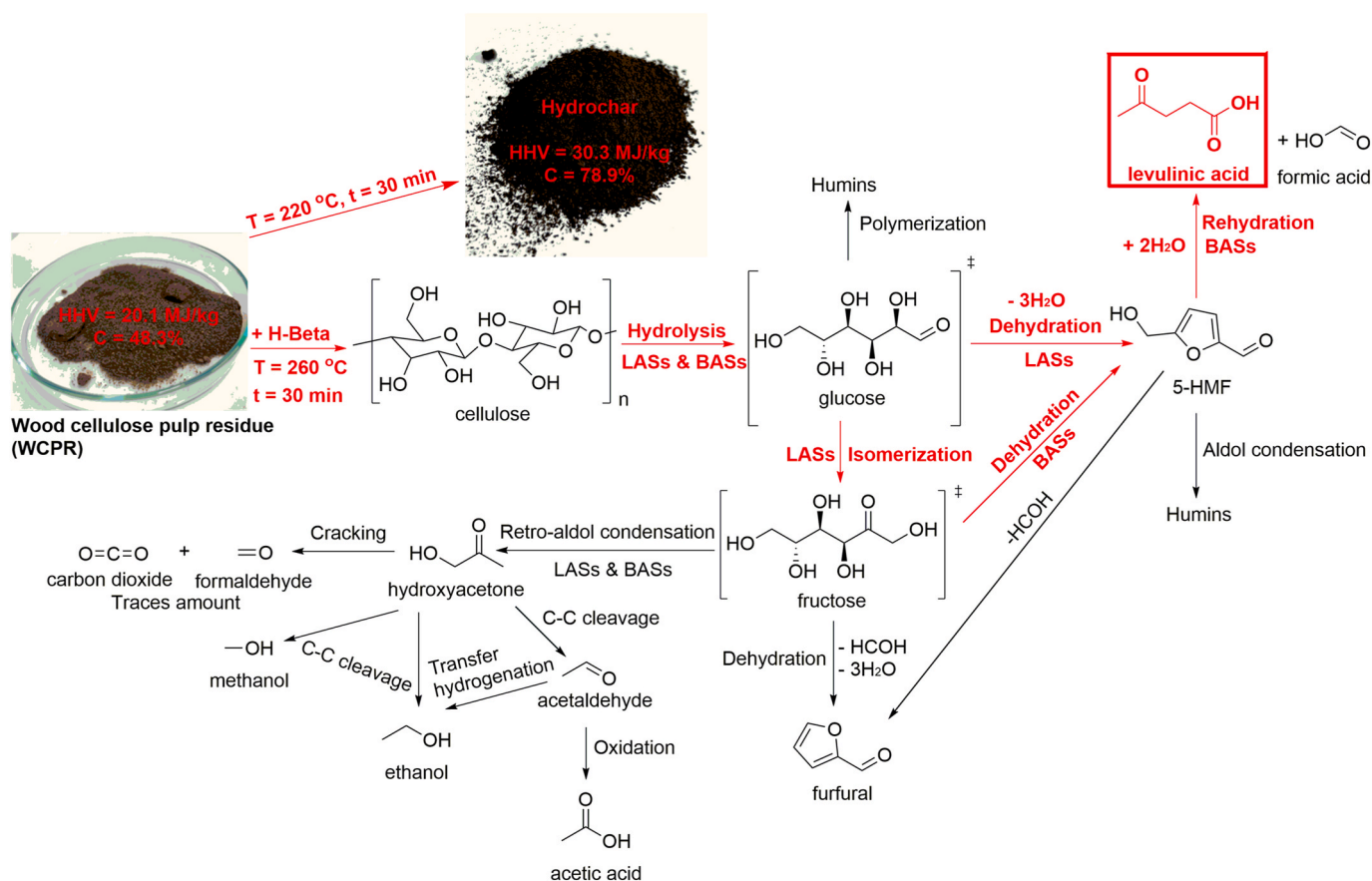


Fig. 10. The reaction pathways for the WT of WCPR with H-Beta zeolite catalyst into hydrochar and the liquid value-added products.

centers, notably Lewis and Brønsted acid sites (LASs and BASs) (Kar-anwal et al., 2022; Ma et al., 2021; Su et al., 2022). Subsequently, glucose undergoes isomerization into fructose over LASs (Song et al., 2019), and this isomerization may also transpire through a hydride shift mechanism involving carbonyl group C1 and hydroxyl group C2 (Ramli and Amin, 2015).

Simultaneously, glucose is subjected to dehydration, leading to the formation of 5-HMF, with active involvement of LASs. Thereafter 5-HMF is subsequently rehydrated into levulinic acid, the primary target compound, alongside the concomitant generation of formic acid. This transformative process is facilitated by BASs, engendering the cleavage of C-C bonds. Under highly acidic conditions, the direct conversion of glucose into levulinic acid, without the intermediary formation of 5-HMF, becomes a plausible pathway. This phenomenon occurs through a cyclic route, with a notable portion of glucose being consumed via the 5-HMF intermediate. As such, the rate-determining step is shifted to the initial dehydration of protonated glucose, thereby promoting the direct conversion of glucose into levulinic acid (Azlan et al., 2022).

The enolate formation simultaneously facilitates the conversion of glucose into fructose (Ma et al., 2021; Ramli and Amin, 2015). Subsequently, fructose undergoes a dehydration reaction, yielding 5-HMF with the involvement of BASs. Fructose eliminates a water molecule to form fructofuranosyloxocarbenium, and this oxocarbenium ion then releases H^+ to generate an enolic compound. The enolic compound undergoes tautomerization before expelling two water molecules to produce 5-HMF. This 5-HMF is subsequently rehydrated in the presence of water within the system. The end products of the rehydration reaction of 5-HMF include levulinic acid and formic acid. Additionally, furfural may be produced within the product mixture due to the release of formaldehyde from the 5-HMF compound (Ramli and Amin, 2015).

Moreover, building upon the identified product distribution, the

plausible formation of hydroxyacetone (acetol) through the retro-aldol condensation of fructose is suggested. Meanwhile, ethanol, methanol, and acetaldehyde are generated as a result of C-C cleavage of hydroxyacetone (Su et al., 2022). Moreover, an extra amount of ethanol can be acquired through the process of acetaldehyde transfer hydrogenation, while acetic acid is produced via the oxidation of acetaldehyde. These findings align with prior research in the literature on specific product outcomes (Song et al., 2019; Wu et al., 2022; Yang et al., 2019). Nonetheless, the formation of humins was observed, as supported by existing literature (Chen et al., 2017; Mikola et al., 2019), which indicates that glucose polymerization and 5-HMF can also produce humins under acid catalysis through aldol condensation with an intermediate compound, 2,5-dioxo-6-hydroxyhexanal. Finally, a small amount of formaldehyde and CO_2 was detected, likely resulting from the cracking of hydroxyacetone.

4. Conclusions

Catalytic wet torrefaction (WT) presents a promising pretreatment method for producing high-quality hydrochar and liquid products. In this work the influence of acid catalyst and reaction conditions on hydrochar properties and liquid product distribution was investigated. The focus was on using wood cellulose pulp residue (WCPR) with the H-Beta zeolite catalyst (0.5–1.5 g) in a nitrogen-rich environment, covering a temperature range from 180 to 260 °C, and reaction durations of 15–60 min. The findings clearly demonstrate that WT conditions, including the use of a WCPR with zeolite catalyst, significantly impact hydrochar properties and the distribution of liquid products. Elemental and proximate analyses revealed substantial changes in hydrochar composition with higher reaction temperature and time, resulting in increased carbon content and decreased oxygen content. The

optimal temperature for levulinic acid production was identified at 260 °C, attaining a remarkable selectivity of 62.8% with 1.0 g of the H-Beta zeolite catalyst and H₂O/WCPR = 10. Additionally, an extensive evaluation was conducted on various hydrochar properties, encompassing HHVs, decarbonization (DC), dehydrogenation (DH), deoxygenation (DO), enhancement factor, carbon enrichment, surface area, pore diameter, and yields of solid, carbon, hydrogen, and energy. The highest carbon content, reaching 78.9%, was achieved at 220 °C after 30 min of treatment for the WT + Beta_220 sample, resulting in an HHV of 30.3 MJ/kg, an enhancement factor of 1.51, and carbon enrichment of 1.63 with the sequence of element removal during WT prioritized as DO > DH > DC. Furthermore, it is noteworthy that the WT + Beta_220 sample exhibits the most substantial weight loss, demonstrating an increase from 17.0 to 60.7%. Conclusively, a comprehensive reaction pathway was suggested to elucidate the interaction between WCPR and the H-Beta zeolite catalyst, shedding light on the reaction mechanism under the optimized conditions. This research underscores WT's potential as a valuable process in biomass waste conversion for sustainable energy and chemical production.

CRedit authorship contribution statement

Andrii Kostyniuk: Writing – review & editing, Writing – original draft, Visualization, Validation, Software, Methodology, Investigation, Formal analysis, Data curation, Conceptualization. **Blaž Likozar:** Supervision, Resources, Project administration, Funding acquisition.

Declaration of competing interest

The authors declare that they have no known competing financial interests or personal relationships that could have appeared to influence the work reported in this paper.

Data availability

Data will be made available on request.

Acknowledgements

The authors express their gratitude for the financial support provided by CARBIOW (Carbon Negative Biofuels from Organic Waste) Research and Innovation Action, which is funded by the European Union under the Horizon Europe Programme, under grant agreement ID: 101084443. The authors would also like to extend their thanks to Urška Kavčič for conducting N₂ physisorption measurements, Dr. Anže Prašnikar for performing SEM analysis, and Mr. Edi Kranjc for conducting XRD analysis. Additionally, they acknowledge the support received from BioTrainValue (BIOmass Valorization via Superheated Steam Torrefaction, Pyrolysis, Gasification Amplified by Multidisciplinary Researchers TRAINing for Multiple Energy and Products' Added VALUEs), with project number: 101086411, funded under Horizon Europe's Maria Skłodowska-Curie Staff Exchange program.

Appendix A. Supplementary data

Supplementary data to this article can be found online at <https://doi.org/10.1016/j.jclepro.2024.141735>.

References

Abdu, H.L., Eid, K., Abdullah, A.M., Han, Z., Ibrahim, M.H., Shan, D., Chen, J., Elzatahry, A.A., Lu, X., 2020. Unveiling one-pot scalable fabrication of reusable carboxylated heterogeneous carbon-based catalysts from eucalyptus plant with the assistance of dry ice for selective hydrolysis of eucalyptus biomass. *Renew. Energy* 153, 998–1004. <https://doi.org/10.1016/j.renene.2020.02.034>.

Alonso, D.M., Gallo, J.M.R., Mellmer, M.A., Wettstein, S.G., Dumesic, J.A., 2013. Direct conversion of cellulose to levulinic acid and gamma-valerolactone using solid acid catalysts. *Catal. Sci. Technol.* 3, 927–931. <https://doi.org/10.1039/c2cy20689g>.

Azlan, N.S.M., Yap, C.L., Gan, S., Rahman, M.B.A., 2022. Recent advances in the conversion of lignocellulosic biomass and its degraded products to levulinic acid: a synergy of Bronsted-Lowry acid and Lewis acid. *Ind. Crops Prod.* 181, 114778. <https://doi.org/10.1016/j.indcrop.2022.114778>.

Bach, Q.V., Chen, W.H., Lin, S.C., Sheen, H.K., Chang, J.S., 2017. Wet torrefaction of microalga *Chlorella vulgaris* ESP-31 with microwave-assisted heating. *Energy Convers. Manag.* 141, 163–170. <https://doi.org/10.1016/j.enconman.2016.07.035>.

Bach, Q.V., Skreiberg, O., 2016. Upgrading biomass fuels via wet torrefaction: a review and comparison with dry torrefaction. *Renew. Sustain. Energy Rev.* 54, 665–677. <https://doi.org/10.1016/j.rser.2015.10.014>.

Chen, D., Cen, K., Chen, F., Zhang, Y., 2022. Solar pyrolysis of cotton stalks: combined effects of torrefaction pretreatment and HZSM-5 zeolite on the bio-fuels upgradation. *Energy Convers. Manag.* 261, 115640. <https://doi.org/10.1016/j.enconman.2022.115640>.

Chen, D., Gao, A., Cen, K., Zhang, J., Cao, X., Ma, Z., 2018. Investigation of biomass torrefaction based on three major components: hemicellulose, cellulose, and lignin. *Energy Convers. Manag.* 169, 228–237. <https://doi.org/10.1016/j.enconman.2018.05.063>.

Chen, S.S., Yu, I.K.M., Tsang, D.C.W., Yip, A.C.K., Khan, E., Wang, L., Ok, Y.S., Poon, C.S., 2017. Valorization of cellulosic food waste into levulinic acid catalyzed by heterogeneous Brønsted acids: temperature and solvent effects. *Chem. Eng. J.* 327, 328–335. <https://doi.org/10.1016/j.cej.2017.06.108>.

Chen, W.H., Fong Eng, C., Lin, Y.Y., Bach, Q.V., Ashokkumar, V., Show, P.L., 2021. Two-step thermodegradation kinetics of cellulose, hemicelluloses, and lignin under isothermal torrefaction analyzed by particle swarm optimization. *Energy Convers. Manag.* 238, 114116. <https://doi.org/10.1016/j.enconman.2021.114116>.

Dai, L., He, C., Wang, Y., Liu, Y., Yu, Z., Zhou, Y., Fan, L., Duan, D., Ruan, R., 2017. Comparative study on microwave and conventional hydrothermal pretreatment of bamboo sawdust: hydrochar properties and its pyrolysis behaviors. *Energy Convers. Manag.* 146, 1–7. <https://doi.org/10.1016/j.enconman.2017.05.007>.

Gan, Y.Y., Ong, H.C., Chen, W.H., Sheen, H.K., Chang, J.S., Chong, C.T., Ling, T.C., 2020. Microwave-assisted wet torrefaction of microalgae under various acids for coproduction of biochar and sugar. *J. Clean. Prod.* 253, 119944. <https://doi.org/10.1016/j.jclepro.2019.119944>.

García, R., Pizarro, C., Lavín, A.G., Bueno, J.L., 2013. Biomass proximate analysis using thermogravimetry. *Bioresour. Technol.* 139, 1–4. <https://doi.org/10.1016/j.biortech.2013.03.197>.

He, C., Tang, C., Li, C., Yuan, J., Tran, K.Q., Bach, Q.V., Qiu, R., Yang, Y., 2018. Wet torrefaction of biomass for high quality solid fuel production: a review. *Renew. Sustain. Energy Rev.* 91, 259–271. <https://doi.org/10.1016/j.rser.2018.03.097>.

He, Q., Raheem, A., Ding, L., Xu, J., Cheng, C., Yu, G., 2021. Combining wet torrefaction and pyrolysis for woody biochar upgradation and structural modification. *Energy Convers. Manag.* 243, 114383. <https://doi.org/10.1016/j.enconman.2021.114383>.

Jian, J., Lu, Z., Yao, S., Li, X., Song, W., 2019. Comparative study on pyrolysis of wet and dry torrefied beech wood and wheat straw. *Energy Fuel.* 33, 3267–3274. <https://doi.org/10.1021/acs.energyfuels.8b04501>.

Karanwal, N., Kurniawan, R.G., Park, J., Verma, D., Oh, S., Kim, S.M., Kwak, S.K., Kim, J., 2022. One-pot, cascade conversion of cellulose to γ -valerolactone over a multifunctional Ru–Cu/zeolite-Y catalyst in supercritical methanol. *Appl. Catal. B Environ.* 314, 121466. <https://doi.org/10.1016/j.apcatb.2022.121466>.

Kostyniuk, A., Bajec, D., Djinović, P., Likozar, B., 2020. One-step synthesis of glycidol from glycerol in a gas-phase packed-bed continuous flow reactor over HZSM-5 zeolite catalysts modified by CsNO₃. *Chem. Eng. J.* 394, 124945. <https://doi.org/10.1016/j.cej.2020.124945>.

Kostyniuk, A., Bajec, D., Djinović, P., Likozar, B., 2020. Allyl alcohol production by gas phase conversion reactions of glycerol over bifunctional hierarchical zeolite-supported bi- and tri-metallic catalysts. *Chem. Eng. J.* 397, 125430. <https://doi.org/10.1016/j.cej.2020.125430>.

Kostyniuk, A., Bajec, D., Likozar, B., 2021a. Catalytic hydrogenation, hydrocracking and isomerization reactions of biomass tar model compound mixture over Ni-modified zeolite catalysts in packed bed reactor. *Renew. Energy* 167, 409–424. <https://doi.org/10.1016/j.renene.2020.11.098>.

Kostyniuk, A., Bajec, D., Likozar, B., 2021b. Catalytic hydrocracking reactions of tetralin as aromatic biomass tar model compound to benzene/toluene/xylenes (BTX) over zeolites under ambient pressure conditions. *J. Ind. Eng. Chem.* 96, 130–143. <https://doi.org/10.1016/j.jiec.2021.01.010>.

Kostyniuk, A., Bajec, D., Likozar, B., 2022. Catalytic hydrocracking reactions of tetralin biomass tar model compound to benzene, toluene and xylenes (BTX) over metal-modified ZSM-5 in ambient pressure reactor. *Renew. Energy* 188, 240–255. <https://doi.org/10.1016/j.renene.2022.01.090>.

Kostyniuk, A., Likozar, B., 2024. Catalytic wet torrefaction of biomass waste into bio-ethanol, levulinic acid, and high quality solid fuel. *Chem. Eng. J.* 485, 149779. <https://doi.org/10.1016/j.cej.2024.149779>.

Kota, K.B., Shenbagaraj, S., Sharma, P.K., Sharma, A.K., Ghodke, P.K., Chen, W.H., 2022. Biomass torrefaction: an overview of process and technology assessment based on global readiness level. *Fuel* 324, 124663. <https://doi.org/10.1016/j.fuel.2022.124663>.

Kwoczyński, Z., Čmelík, J., 2021. Characterization of biomass wastes and its possibility of agriculture utilization due to biochar production by torrefaction process. *J. Clean. Prod.* 280, 124302. <https://doi.org/10.1016/j.jclepro.2020.124302>.

Leontiev, A., Kichatov, B., Korshunov, A., Kiverin, A., Zaichenko, V., Sytchev, G., Melnikova, K., 2018. Oxidative torrefaction of pine pellets in the quiescent layer of

- mineral filler. *Fuel Process. Technol.* 182, 113–122. <https://doi.org/10.1016/j.fuproc.2018.10.021>.
- Li, M., Wang, H., Huang, Z., Yuan, X., Tan, M., Jiang, L., Wu, Z., Qin, X., Li, H., 2020. Comparison of atmospheric pressure and gas-pressurized torrefaction of municipal sewage sludge: properties of solid products. *Energy Convers. Manag.* 213, 112793 <https://doi.org/10.1016/j.enconman.2020.112793>.
- Li, M.F., Shen, Y., Sun, J.K., Bian, J., Chen, C.Z., Sun, R.C., 2015. Wet torrefaction of bamboo in hydrochloric acid solution by microwave heating. *ACS Sustain. Chem. Eng.* 3, 2022–2029. <https://doi.org/10.1021/acssuschemeng.5b00296>.
- Li, X., Lu, Z., Chen, J., Chen, X., Jiang, Y., Jian, J., Yao, S., 2021. Effect of oxidative torrefaction on high temperature combustion process of wood sphere. *Fuel* 286, 119379. <https://doi.org/10.1016/j.fuel.2020.119379>.
- Li, X., Xu, R., Yang, J., Nie, S., Liu, D., Liu, Y., Si, C., 2019. Production of 5-hydroxymethylfurfural and levulinic acid from lignocellulosic biomass and catalytic upgradation. *Ind. Crops Prod.* 130, 184–197. <https://doi.org/10.1016/j.indcrop.2018.12.082>.
- Lin, Y.L., Zheng, N.Y., Hsu, C.H., 2021. Torrefaction of fruit peel waste to produce environmentally friendly biofuel. *J. Clean. Prod.* 284, 124676 <https://doi.org/10.1016/j.jclepro.2020.124676>.
- Ma, C., Cai, B., Zhang, L., Feng, J., Pan, H., 2021. Acid-catalyzed conversion of cellulose into levulinic acid with biphasic solvent system. *Front. Plant Sci.* 12 <https://doi.org/10.3389/fpls.2021.630807>.
- Ma, Q., Han, L., Huang, G., 2018. Effect of water-washing of wheat straw and hydrothermal temperature on its hydrochar evolution and combustion properties. *Bioresour. Technol.* 269, 96–103. <https://doi.org/10.1016/j.biortech.2018.08.082>.
- Mikola, M., Ahola, J., Tanskanen, J., 2019. Production of levulinic acid from glucose in sulfolane/water mixtures. *Chem. Eng. Res. Des.* 148, 291–297. <https://doi.org/10.1016/j.cherd.2019.06.022>.
- Missouli, A., Bostyn, S., Belandria, V., Cagnon, B., Sarh, B., Gökalp, I., 2017. Hydrothermal carbonization of dried olive pomace: energy potential and process performances. *J. Anal. Appl. Pyrolysis* 128, 281–290. <https://doi.org/10.1016/j.jaap.2017.09.022>.
- Niu, X., Xu, Y., Shen, L., 2022. Effect of torrefaction on the evolution of carbon and nitrogen during chemical looping gasification of rapeseed cake. *Chem. Eng. J.* 450, 138134 <https://doi.org/10.1016/j.cej.2022.138134>.
- Ong, H.C., Chen, W.H., Singh, Y., Gan, Y.Y., Chen, C.Y., Show, P.L., 2020. A state-of-the-art review on thermochemical conversion of biomass for biofuel production: a TG-FTIR approach. *Energy Convers. Manag.* 209, 112634 <https://doi.org/10.1016/j.enconman.2020.112634>.
- Ramli, N.A.S., Amin, N.A.S., 2015. Optimization of renewable levulinic acid production from glucose conversion catalyzed by Fe/HY zeolite catalyst in aqueous medium. *Energy Convers. Manag.* 95, 10–19. <https://doi.org/10.1016/j.enconman.2015.02.013>.
- Rodríguez-Alejandro, D.A., Nam, Hoseok, Granados-Lieberman, D., Wang, S., Hwang, S. C., Nam, Hyungseok, Capareda, S.C., 2023. Experimental and numerical investigation on a solar-driven torrefaction reactor using woody waste (Ashe Juniper). *Energy Convers. Manag.* 288, 117114 <https://doi.org/10.1016/j.enconman.2023.117114>.
- Saha, N., Fillerup, E., Thomas, B., Pilgrim, C., Causer, T., Herren, D., Klinger, J., 2022. Improving bamboo's fuel and storage properties with a net energy export through torrefaction paired with catalytic oxidation. *Chem. Eng. J.* 440, 135750 <https://doi.org/10.1016/j.cej.2022.135750>.
- Sarvaramini, A., Assima, G.P., Larachi, F., 2013. Dry torrefaction of biomass - torrefied products and torrefaction kinetics using the distributed activation energy model. *Chem. Eng. J.* 229, 498–507. <https://doi.org/10.1016/j.cej.2013.06.056>.
- Song, H., Wang, P., Li, S., Deng, W., Li, Y., Zhang, Q., Wang, Y., 2019. Direct conversion of cellulose into ethanol catalysed by a combination of tungstic acid and zirconia-supported Pt nanoparticles. *Chem. Commun.* 55, 4303–4306. <https://doi.org/10.1039/c9cc00619b>.
- Srisang, S., Phetpan, K., Ruttanadech, N., Limmun, W., Youryon, P., Kongtragoul, P., Srisang, N., Chungcharoen, T., 2022. Charcoal briquette production from waste in the coffee production process using hydrothermal and torrefaction techniques: a comparative study with carbonization technique. *J. Clean. Prod.* 372, 133744 <https://doi.org/10.1016/j.jclepro.2022.133744>.
- Statista Research Department, 2023. Production of Wood Pulp Worldwide from 1961 to 2022 [WWW Document]. URL: <https://www.statista.com/statistics/240570/consumption-and-production-of-fibrous-material-worldwide/>.
- Su, Z., Zhang, J., Lu, S., Xiao, F.S., 2022. Pt nanoparticles supported on Nb-modified TiO₂ as an efficient heterogeneous catalyst for the conversion of cellulose to light bioalcohols. *Chem. Commun.* 58, 12349–12352. <https://doi.org/10.1039/d2cc03845e>.
- Sukiran, M.A., Abnisa, F., Wan Daud, W.M.A., Abu Bakar, N., Loh, S.K., 2017. A review of torrefaction of oil palm solid wastes for biofuel production. *Energy Convers. Manag.* 149, 101–120. <https://doi.org/10.1016/j.enconman.2017.07.011>.
- Tong, S., Xiao, L., Li, X., Zhu, X., Liu, H., Luo, G., Worasuwannarak, N., Kerdsuwan, S., Fungtammanan, B., Yao, H., 2018. A gas-pressurized torrefaction method for biomass wastes. *Energy Convers. Manag.* 173, 29–36. <https://doi.org/10.1016/j.enconman.2018.07.051>.
- Volpe, M., Fiori, L., 2017. From olive waste to solid biofuel through hydrothermal carbonisation: the role of temperature and solid load on secondary char formation and hydrochar energy properties. *J. Anal. Appl. Pyrolysis* 124, 63–72. <https://doi.org/10.1016/j.jaap.2017.02.022>.
- Wang, K., Jiang, J., Liang, X., Wu, H., Xu, J., 2018. Direct conversion of cellulose to levulinic acid over multifunctional sulfonated humins in sulfolane-water solution. *ACS Sustain. Chem. Eng.* 6, 15092–15099. <https://doi.org/10.1021/acssuschemeng.8b03558>.
- Weingarten, R., Conner, W.C., Huber, G.W., 2012. Production of levulinic acid from cellulose by hydrothermal decomposition combined with aqueous phase dehydration with a solid acid catalyst. *Energy Environ. Sci.* 5, 7559. <https://doi.org/10.1039/c2ee21593d>.
- Wu, N., Niu, Q., Pieters, J., Ronsse, F., 2023. Influence of torrefaction as pretreatment on the fast pyrolysis of sugarcane trash. *Energy Convers. Manag.* 291, 117291 <https://doi.org/10.1016/j.enconman.2023.117291>.
- Wu, Y., Dong, C., Wang, H., Peng, J., Li, Y., Samart, C., Ding, M., 2022. One-pot ethanol production from cellulose transformation over multifunctional Pt/WOx and hollow Pt@HZSM-5 catalysts. *ACS Sustain. Chem. Eng.* 10, 2802–2810. <https://doi.org/10.1021/acssuschemeng.1c08204>.
- Xiang, M., Liu, J., Fu, W., Tang, T., Wu, D., 2017. Improved activity for cellulose conversion to levulinic acid through hierarchization of ETS-10 zeolite. *ACS Sustain. Chem. Eng.* 5, 5800–5809. <https://doi.org/10.1021/acssuschemeng.7b00529>.
- Xu, X., Liang, B., Zhu, Y., Chen, J., Gan, T., Hu, H., Zhang, Y., Huang, Z., Qin, Y., 2023. Direct and efficient conversion of cellulose to levulinic acid catalyzed by carbon foam-supported heteropolyacid with Brønsted–Lewis dual-acidic sites. *Bioresour. Technol.* 387, 129600 <https://doi.org/10.1016/j.biortech.2023.129600>.
- Yang, M., Qi, H., Liu, F., Ren, Y., Pan, X., Zhang, L., Liu, X., Wang, H., Pang, J., Zheng, M., Wang, A., Zhang, T., 2019. One-pot production of cellulosic ethanol via tandem catalysis over a multifunctional Mo/Pt/WOx catalyst. *Joule* 3, 1937–1948. <https://doi.org/10.1016/j.joule.2019.05.020>.
- Zhang, C., Ho, S.H., Chen, W.H., Fu, Y., Chang, J.S., Bi, X., 2019. Oxidative torrefaction of biomass nutshells: evaluations of energy efficiency as well as biochar transportation and storage. *Appl. Energy* 235, 428–441. <https://doi.org/10.1016/j.apenergy.2018.10.090>.
- Zhang, C., Ho, S.H., Chen, W.H., Xie, Y., Liu, Z., Chang, J.S., 2018. Torrefaction performance and energy usage of biomass wastes and their correlations with torrefaction severity index. *Appl. Energy* 220, 598–604. <https://doi.org/10.1016/j.apenergy.2018.03.129>.
- Zhang, C., Wang, M., Chen, W.H., Pétrissans, A., Pétrissans, M., Ho, S.H., 2022. A comparison of conventional and oxidative torrefaction of microalga *Nannochloropsis Oceanica* through energy efficiency analysis and life cycle assessment. *J. Clean. Prod.* 369, 133236 <https://doi.org/10.1016/j.jclepro.2022.133236>.
- Zhang, S., Chen, T., Xiong, Y., Dong, Q., 2017. Effects of wet torrefaction on the physicochemical properties and pyrolysis product properties of rice husk. *Energy Convers. Manag.* 141, 403–409. <https://doi.org/10.1016/j.enconman.2016.10.002>.
- Zhang, X., Guo, J., Yu, Y., Hao, X., Xu, Y., Yao, Q., Guo, Y., 2023. Preparation of Pectin Lyase by fermentation for customized extraction of paper pulp, viscose fiber, and nanofibrillated cellulose from hemp stalks. *Ind. Crops Prod.* 203 <https://doi.org/10.1016/j.indcrop.2023.117137>.
- Zhu, L., Hu, Z., Huang, M., Peng, H., Zhang, W., Chen, D., Ma, Z., 2022. Valorisation of cotton stalk toward bio-aromatics: effect of wet torrefaction deoxygenation and demineralization pretreatment on catalytic fast pyrolysis using Ga modified hierarchical zeolite. *Fuel* 330, 125571. <https://doi.org/10.1016/j.fuel.2022.125571>.
- Zhu, Xiefei, Luo, Z., Diao, R., Zhu, Xifeng, 2019. Combining torrefaction pretreatment and co-pyrolysis to upgrade biochar derived from bio-oil distillation residue and walnut shell. *Energy Convers. Manag.* 199, 111970 <https://doi.org/10.1016/j.enconman.2019.111970>.